JAERI-M
9495

FRETA-B: A COMPUTER CODE FOR THE ANALYSIS OF FUEL ROD BUNDLE BEHAVIORS UNDER ACCIDENT CONDITIONS

May 1981

Masaaki UCHIDA, Jinichi NAKAMURA
and Naoaki OTSUBO*

日本原子力研究所
Japan Atomic Energy Research Institute

この報告書は，日本原子力研究所がJAERI-Mレポートとして，不定期に刊行している研究報告書です．入手，複製などのお問合わせは，日本原子力研究所技術情報部（茨城県那珂郡東海村）あて，お申しこしください．

JAERI-M reports, issued irregularly, describe the results of research works carried out in JAERI. Inquiries about the availability of reports and their reproduction should be addressed to Division of Technical Information, Japan Atomic Energy Research Institute, Tokai-mura, Naka-gun, Ibaraki-ken, Japan.

JAERI-M 9495

FRETA-B : A Computer Code for the Analysis of Fuel Rod Bundle Behaviors under Accident Conditions

Masaaki UCHIDA, Jinichi NAKAMURA and Naoaki OTSUBO*

Division of Nuclear Fuel Research, Tokai Research Establishment, JAERI

(Received April 27, 1981)

A two-dimensional code FRETA-B was developed to analyze the behaviors of LWR fuel rod bundles under accident conditions. It calculates fuel temperatures, oxidation of claddings, plenum gas pressure and flow, and deformations of fuel rods.

Two-dimensional treatment is made in the transverse direction: a fuel rod bundle, or its part, is represented by several discrete cross-sections at different elevations. Most submodels treat each azimuthal sector of each rod independently, but the radiant heat transfer submodel treats all rods simultaneously. Also, two-dimensional treatment is made in each rod on the ballooning and the collapse of the cladding.

This paper describes the models and gives an input manual of the code.

Keywords: Fuel, LWR, Bundle, Analysis, Code, FRETA-B, Two-Dimentional Calculations, Reactor Safety

---

* Century Research Center Corp.

FRETA－B：事故時燃料バンドル挙動解析コード

日本原子力研究所東海研究所安全工学部

内田正明・中村仁一・大坪直昭*

（1981年4月27日受理）

事故時の軽水炉燃料バンドル挙動解析のため，2次元コードFRETA－Bを開発した。本コードは燃料各部の温度，被覆管の酸化，プレナムガスの圧力と流れ，および燃料棒の変形を計算する。

2次元化は横断面方向に行い，1体の燃料バンドルまたは，その小部分を軸方向数ケ所における互いに独立な横断面によって代表させている。多くのサブモデルは，燃料棒を周方向に分割するセクターを独立に扱うが，輻射伝熱のサブモデルにおいてはすべての燃料棒およびセクターを同時に扱っている。また，被覆管のバルーニングとコラプスについては，燃料棒毎に2次元的な扱いをしている。

本報告は計算モデルを記述するとともに，入力方法の手引を記載している。

* センチュリ・リサーチ・センター（株）

CONTENTS

目　　次

1. INTRODUCTION

FRETA-B (Fuel Reliability Evaluation Code for Transient and Accident-Bundle Geometry) is a transient fuel behavior analysis code, which deals with bundles of Zircaloy-clad oxide fuel rods in light water reactors. It is aimed at analyzing the behaviors under accident conditions, especially loss-of-coolant accident (LOCA).

The code is in fact the third version in a series of development work for the purpose. The first version in this series was FREG-3T[1], which was virtually a modification of a steady-state fuel thermal analysis code FREG-3 for the transient analysis purpose. The modification required fuel rod surface heat transfer models and high-temperature materials property data. They were mostly taken from the US hydraulic code RELAP-4[2] and the materials data package MATPRO[3].

The step to the next version included only small modifications; some improvements were made on pellet-cladding interaction (PCI) and surface heat transfer models. The code name was changed to FRETA. Both FREG-3T and FRETA were single-rod codes with axisymmetric models, aiming at best estimation.

Expansion into a two-dimensional code treating a (part of) fuel rod bundle was motivated by a recent experimental finding[4] that the baloon-ing and rupture behaviors of cladding are affected by azimuthal temperature gradient. The gradient, unavoidable even in single-rod experiments, is very large in test bundles with small number of fuel rods. Thus, apart from the discussion whether the temperature gradient is singnificant in power reactors or not, the two-dimensional treatment was required for verifying the code against various simulation experiments.

FRETA-B is a bundle code, not a mere stack of single rod routines, because it treats multiple rods simultaneously in calculating radiant heat transfer. It also considers the effect of local flow area reduction on the input coolant state, but the treatment is still preliminary. In each rod, two-dimensional treatment is made for the ballooning of claddings. Also, a corrective calculation is made to account for transverse heat flow in a rod. With other submodels, one-dimensional treatment is made in each fuel sector which divides a fuel cross section into four.

Figure 1 lists main subroutines of FRETA-B to show the scope and flow of its calculation. Figure 2 also serves for the same purpose, but main submodels instead of subroutines are classified according to the

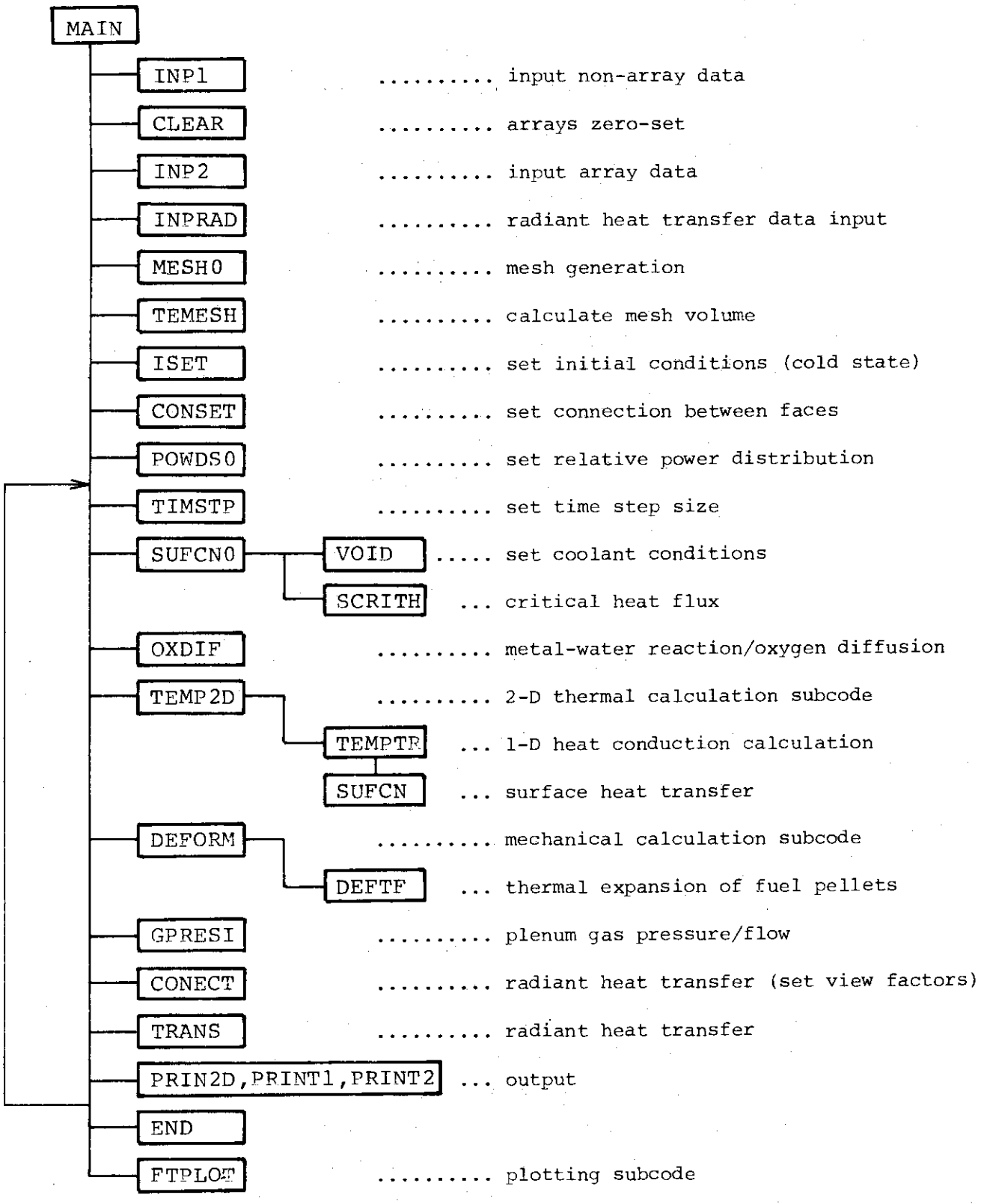

Fig. 1 Flow of calculation in FRETA-B

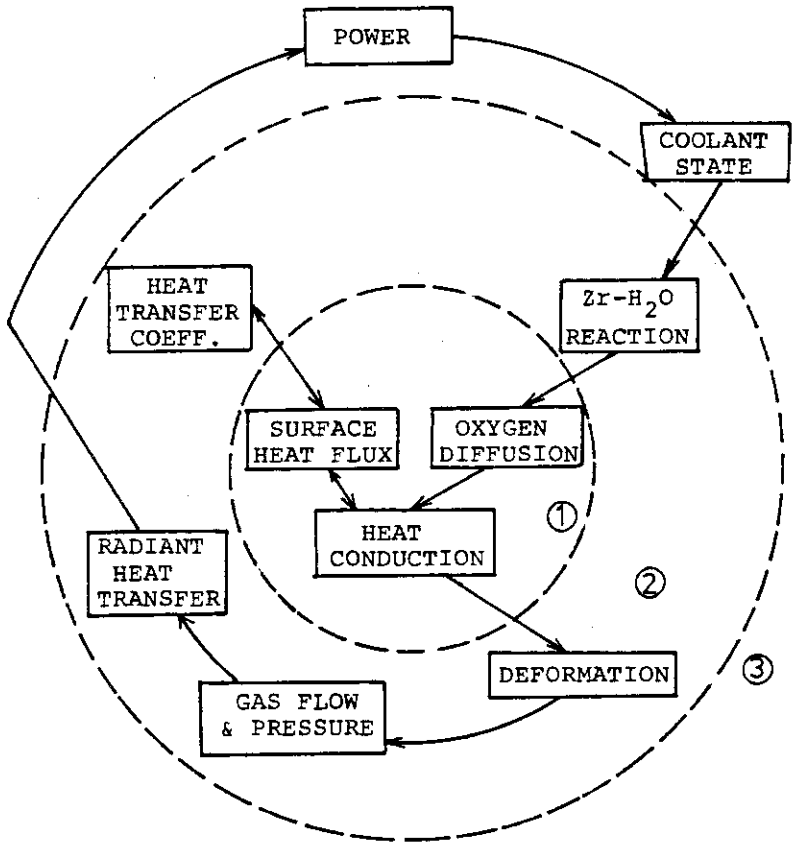

Fig. 2 Flow of calculation with submodels classified according to the solution method: Zone 1 Krank-Nicolson's semiexplicit method, zone 2 explicit solution, zone 3 input.

solution methods of their main equations. In the innermost circle of the figure, the Krank-Nicolson's semi-explicit finite-difference formulation is used only for fuel rod internal heat conduction equations which are solved simultaneously with convective surface heat transfer equations, and for oxygen diffusion equation in the cladding.

For the other models in the second circle, more time-saving explicit formulations are used. No iteration is made in a subcode, nor between different subcodes: a calculation run always proceed forward. Stability problems are circumvented partly by limiting fuel temperature increments in each time step within a certain limit. If the limit is exceeded, the current time step is canceled and the time step size is reduced to one half.

As a transient code, FRETA-B does not calculate by itself any fuel state change that proceed slowly during steady reactor operations. Figure 3 shows how FRETA-B accounts for these fuel state changes calculated by other steady codes. An imaginary cold state is postulated at -2000 sec

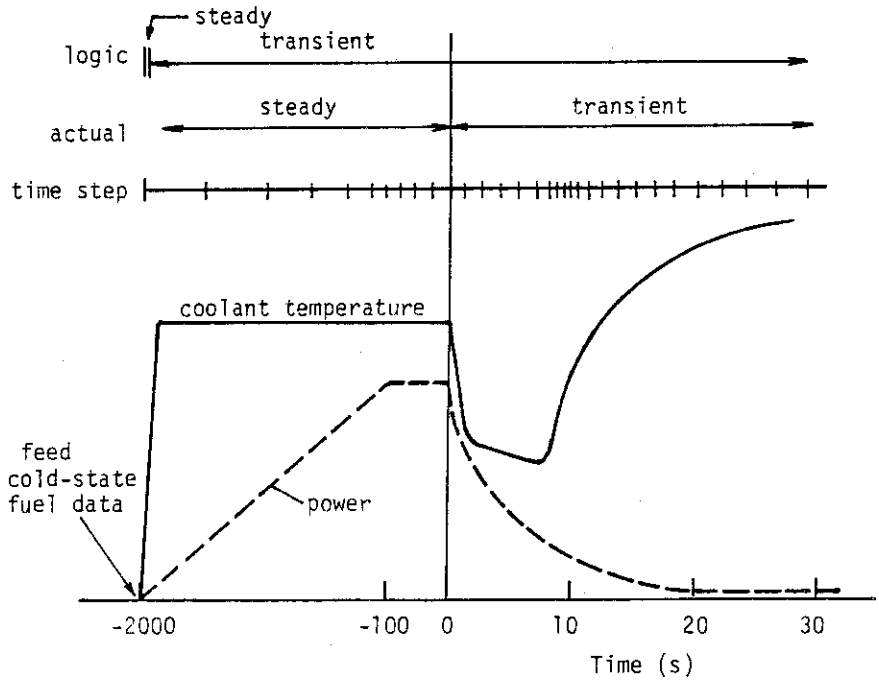

Fig. 3 Treatment of the steady state before transient by FRETA-B

from the onset of transient, and the state changes are input to the code as describing the cold state at the period. Then an imaginary ramp is made to the actual steady state at time zero. From the calculational logic, this ramp is also treated as a transient.

The maximum size of bundle geometry can be easily expanded, of cource at the expense of necessary core memory and calculation time. The present standard size is 10 fuel rods, 10 axial segments, 9 radial rings and fixed 4 azimuthal sectors of each rod.

2. GEOMETRICAL MODEL

FRETA-B treats a complete, or part of square-lattice fuel bundle. The geometry is reduced using the symmetry in the cross-section of a bundle. The reduced bundle will hereafter be called 'partial bundle'. In the axial direction, whole length of fuel rods is divided into axial segments. A fuel rod is modelled as composed of a stack of identical fuel pellets and the cladding, with upper and lower plena: fuel rod spacers are not modelled in the present version.

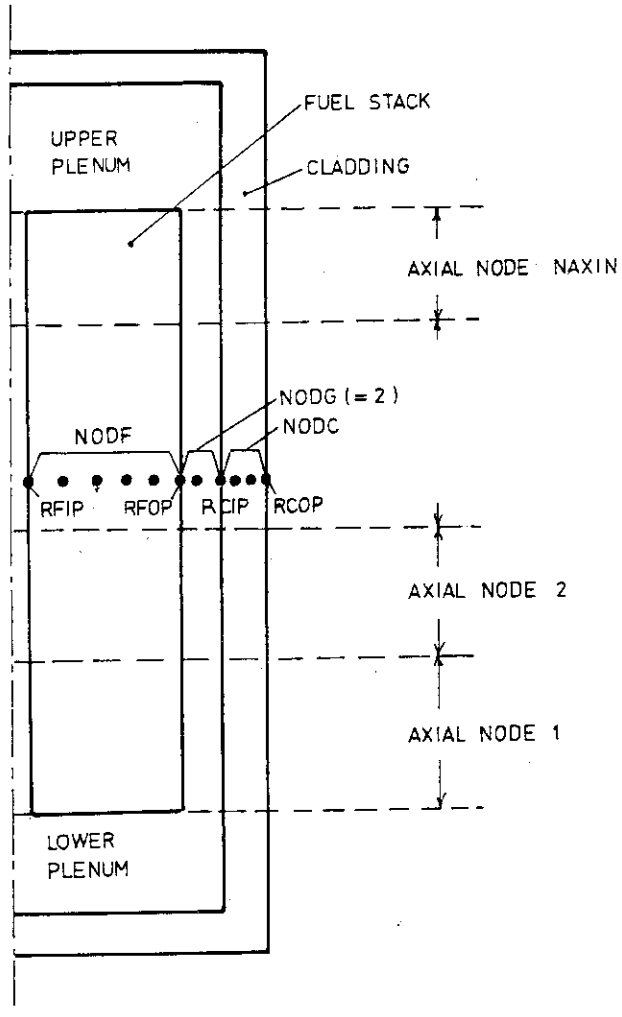

Fig. 4 Nodalization of a fuel rod

Axial segments can have either identical or different length, depending on the purpose of the analysis. A segment is primarily independent of the others except in a few models, e.g., axial gas flor and the coolant enthalpy rise.

The radial power distribution (fractional) must be the same in all

the axial segments. The initial geometry must also be the same, but provisions are made to account for the axially-variant 'initial strains' such as fuel swelling or cladding creepdown, which had taken place during steady reactor operations before the transient.

Thus the cross-sectional geometry of a partial bundle is fundamentally common to all the axial segments. Figure 5 shows examples of cross sections. Different from axial segmentation, the cross sectional geometry is additive or modular, i.e., a partial bundle with arbitrary geometry and size can be composed by a user combining 'unit cells'.

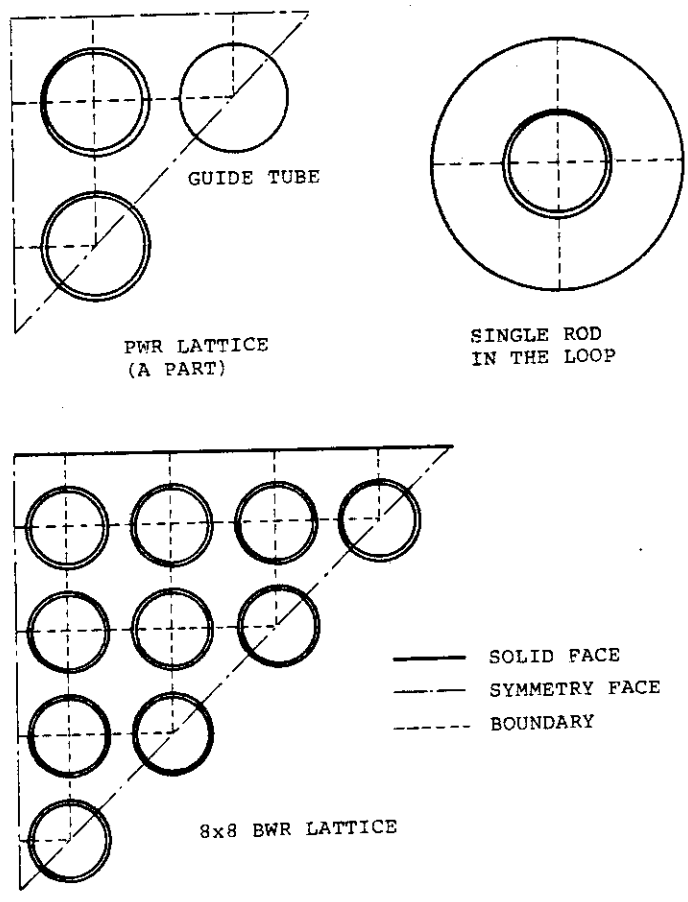

Fig. 5 Examples of partial bundle geometry

Each fuel rod is divided into four azimuthal sectors. A unit cell is composed of a coolant subchannel and four surrounding fuel sectors, in some cases also shroud and symmetry faces. Each fuel sector is primarily independent of the others and, divided into radial rings, analyzed one-dimensionally except in a few sub-models.

Consider as an example the partial bundle of Fig. 6. It is a 1/8 sector of a symmetrical 3 × 3 lattice. Three unit cells define the whole

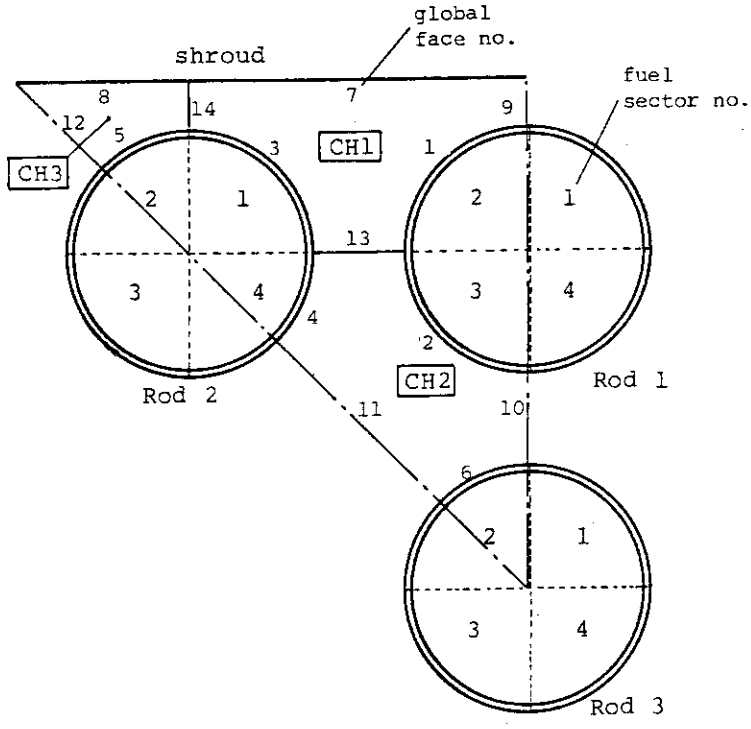

Fig. 6 Example of sequential numbers defining the geometry (used for the sample input list in Table A5 of the APPENDIX)

geometry. In this example, no rod is completely within the partial bundle, all located on the symmetry faces.

Four sectors of a rod have counter-clockwise sequential numbers. The sequence includes also the sector which is outside a symmetry face, i.e., outside the partial bundle. The code recognizes that odd-odd or even-even pairs of sector numbers are diagonal.

Geometrical relationship between fuel sectors of different fuel rods is indintified by specifying the correspondence between fuel rod sector number, global face element number and local face number in a unit cell. Three types of unit cell are used to define the partial bundle of Fig. 6. In each type, the local face number sequence is determined as in Fig. 7. All the face elements in the partial bundle, including the boundaries between subchannels, are given global through numbers. Relationships between them are specified by input:

fuel rod no. / sector no. → global face no. → { subchannel no. / unit cell type / local face no.

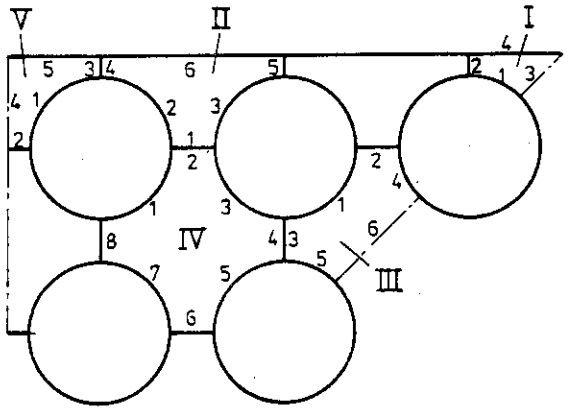

Fig. 7 Subchannel type number (Roman numerals) and local face number (Arabic numerals)

Thus the geometrical relationship between two fuel sectors, facing the same subchannel, is identified from their local face numbers, and the thermal interaction between the sectors is treated using their global face numbers.

Part of the external boundary may be a shroud face. A shroud plate is modelled as a zero-thickness plate in thermal equilibrium with the coolant, lying a half-pitch distance apart from the center of the outermost rod raw. Water rods and control-rod guide tubes are also treated as 'shrouds' with cylindrical geometry: since their effects on fuel rods are, in the present models, merely to emmit and absorb radiation energy, it is not necessary to distinguish them.

3. THERMAL MODELS

3.1 Scope

Heat transfer calculation are performed

1) inside fuel rods,
2) between fuel rod and the coolant (convective), and
3) between fuel rods, and between a rod and the coolant (radiant).

The phenomena 1) and 2) are treated simultaneously in each rod, but 3) is separately calculated and the results are treated as additive heat source terms in the next time step.

The convective heat transfer depends very much on the coolant states, which usually change drastically during a cource of accident. For necessary coolant state data, FRETA-B depends on the calculations by reactor thermo-hydraulic codes or experimental data. FRETA-B has five options for setting the boundary condition:

MODSHT=1	cladding temperature history is input,
MODSHT=2	axially uniform enthalpy and mass flux histories are input,
MODSHT=3	coolant state history at the inlet and outlet to the core is input,
MODSHT=4	coolant temperature and heat transfer coefficient histories at each axial node are input,
MODSHT=5	coolant enthalpy and mass flux histories at each axial node are input.

The coolant pressure history data are required in all cases. With MODSHT=3, local enthalpy at an axial node is calculated from the inlet enthalpy and mass flux, assuming stationary coolant states. Therefore, it is not applicable to the case with rapid coolant state changes, especially under reversal of flow direction.

FRETA-B makes no hydraulic calculation by itself. All the coolant subchannels are assumed to have identical enthalpy and mass flux at an elevation. With the options MODSHT=2, or 5, however, an option for corrective mass flux calculation is provided: when large ballooning of the claddings resulted in local flow area reduction, the input mass flux is redistributed among subchannels according to local flow resistances.

The radiant heat transfer model is fully two-dimensional. Other

models are one-dimensional in each fuel sector. But the fuel center temperature of each rod, which takes four different values after a series of sectorwise calculation, is averaged to a single value. This calculation cycle corresponds to treating heat flow across the center.

3.2 Heat Source Terms

Heat sources considered in FRETA-B are, 1) prompt fission heat, 2) delayed fission heat, 3) decay heat after shutdown, and 4) metal-water reaction heat in the cladding. The last one is calculated separately and described in Chapter 4. For the first three, three input options are provided:

1) total power history table is input,
2) delayed fission heat is calculated and used together with the stored ANS 1978 standard table for decay heat,
3) The ANS standard table is used alone with a multiplication factor of 1.2.

The relevant part of the ANS standard[5] is shown in Table 1, where infinite duration of irradiation is assumed. When options 2) and 3) are used, the power level at the onset of transient is input, and Table 1 data are used fractionally assuming the fission power of 200 MeV.

Delayed fission power is given as a fraction to the initial prompt fission power p_0 by

$$P_n(t) = P_1 \sum_{i}^{6} [A_i \exp(-t/\tau_i)] \tag{3.1}$$

$$\frac{P_1}{P_0} = \frac{\beta}{\beta + \rho_{sm}} \tag{3.2}$$

where $P_n(t)$ is delayed fission heat, β is the fraction of total delayed neutron (0.007). Scram reactivity ρ_{sm} differs from reactor to reactor and can be input. The terms A_i and τ_i are the fraction and half life, respectively, of the i-th precurser nuclide and stored in the code.

Heat generation rate from the above sources is expressed in the form

$$P(n,\theta,r,z,t) = \bar{P}_0(n) \cdot f(\theta,n) \cdot g(r) \cdot h(z) \cdot p(t) \tag{3.3}$$

where n is rod number, θ represents azimuthal sectors, r is radius, z is

Table 1 ANS 1978 standard decay heat table (^{235}U, 10^{13}s irradiation)

Time After Shutdown (s)	Decay Heat Power F(t,∞) (MeV/fission)
1.0000E+00	1.231E+01
1.5000E+00	1.198E+01
2.0000E+00	1.169E+01
4.0000E+00	1.083E+01
6.0000E+00	1.026E+01
8.0000E+00	9.830E+00
1.0000E+01	9.494E+00
1.5000E+01	8.882E+00
2.0000E+01	8.455E+00
4.0000E+01	7.459E+00
6.0000E+01	6.888E+00
8.0000E+01	6.493E+00
1.0000E+02	6.198E+00
1.5000E+02	5.696E+00
2.0000E+02	5.369E+00
4.0000E+02	4.667E+00
6.0000E+02	4.282E+00
8.0000E+02	4.009E+00
1.0000E+03	3.796E+00
1.5000E+03	3.408E+00
2.0000E+03	3.137E+00
4.0000E+03	2.534E+00
6.0000E+03	2.234E+00
8.0000E+03	2.044E+00
1.0000E+04	1.908E+00

axial elevation (segments) and t is time. $P_0(n)$ is the average linear heat rating of rod n at time zero. Equation (3.3) means that sectorwise power fraction can be given independently in each rod, but that axial and radial power distribution (relative) are common to all rods and also the time dependency is common to every local power.

3.3 Convective Heat Transfer at the Cladding Surface

Convective heat transfer equation is solved simultaneously with the internal heat conduction equation successively in each fuel sector. Except under options MODSHT=1 or 4, calculation starts from setting the local instantaneous coolant state from the input history data.

Under options MODSHT=2 and 5, a set of enthalpy, pressure and mass flux data is allocated to each axial node.

Under option MODSHT=3, local enthalpy at n-th axial node from inlet (or outlet if the outlet enthalpy is lower) is calculated assuming stationary flow and power production as

$$H = H_{in} + \sum_{i=1}^{n} \frac{q_i^m S_i}{GA} \tag{3.4}$$

where H_{in} is inlet (or outlet) enthalpy, q_i^m is heat flux at axial node i in the previous time step, A is flow area, S_i is conductive surface area in segment i, and G is mass flux.

The coolant enthalpy and pressure data set is compared with the steam table and the phase and temperature are determined. In the two-phase state, quality and void fraction are calculated by

$$X = (H - H_f)/(H_g - H_f) \tag{3.5}$$

$$\alpha = \frac{X\, v_g}{(1-X)\, v_f + X\, v_g} \tag{3.6}$$

where X and α are quality and void fraction, respectively, H is enthalpy, v is specific volume and suffices g and f mean saturated steam and fluid, respectively. Thermal conductivity and viscosity data are also referred to the table.

Boiling curve is modelled as Fig. 8. It is composed of seven different relationships (modes) between the cladding wall temperature and heat flux. One out of them is selected according to the state or from

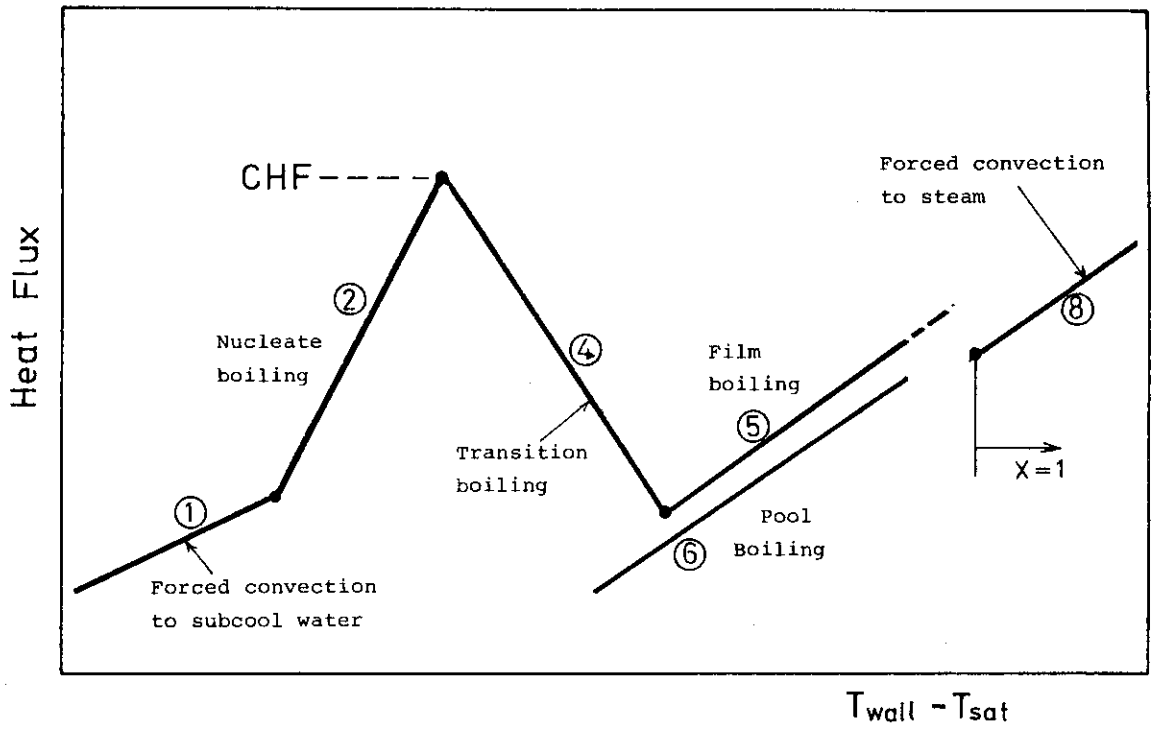

Fig. 8 Boiling curve model and heat transfer correlations (The mode number is attached to each curve.)

the comparison between the magnitudes of heat flux they give. The heat transfer correlations as well as the logic tree to select one of them was taken from RELAP4 MOD5[2] (some were discarded) as stated below. Nomenclature is listed up at the end of this section.

Mode 1 forced convection to subcooled water (Dittus-Boelter)

$$h = 0.023 \frac{k}{De} \mathrm{Pr}^{0.4} \cdot \mathrm{Re}^{0.8} \tag{3.7}$$

Mode 2 nucleate boiling (Thom)

$$q = \left[\frac{(T_w - T_{sat}) \exp(P/1260)}{0.072}\right]^2 \tag{3.8}$$

Mode 4 transition boiling (McDonough-Milich-King)

$$q = q_{CHF} - C(P)\ (T_w - T_{w,CHF}) \tag{3.9}$$

where q_{CHF} is critical heat flux, and $T_{w,CHF}$ is the corresponding wall temperature in Mode 2, namely, the temperature derived by substituting q_{CHF} into the term q in (3.8). $C(P)$ is a pressure-dependent coefficient

given by the following table

P (psi)	$C(P)$
2000	979.2
1000	1180.8
800	1501.2

Mode 5 stable film boiling (Groeneveld)

$$h = 0.00327 \frac{K_g}{D_e} \mathrm{Pr}_f^{1.32} [\mathrm{Re}_g \{X + \frac{\rho_g}{\rho_f} (1 - X)\}]^{0.901}$$

$$\{1.0 - 0.1(1 - X)^{0.4} (\frac{\rho_f}{\rho_g} - 1)^{0.4}\}^{-1.5} \qquad (3.10)$$

Mode 6 laminar pool boiling (Berenson)

$$q = F(P) \ (T_w - T_{sat})^{3/4} \qquad (3.11)$$

Mode 8 forced convection to superheated steam (Dittus-Boelter)

same in form as (3.7) but with steam properties.

Mode 9 low pressure film boiling (Dougall-Rohsenow)

$$h = 0.023 \frac{K_g}{D_e} \mathrm{Pr}_g^{0.4} [\mathrm{Re}_g \{X + \frac{\rho_g}{\rho_f} (1 - X)\}]^{0.8} \qquad (3.12)$$

Nomenclature is:

- q = heat flux (Btu/ft^2 hr)
- h = heat transfer coefficient (Btu/ft^2 °F hr)
- T = temperature (°F)
- P = pressure (lb/in^2)
- ρ = density (lb/ft^3)
- x = quality
- D_e = equivalent hydraulic diameter (in)
- Re = Reynolds number
- Pr = Prantdl number
- k = thermal conductivity (Btu/ft °F)
- μ = viscosity (lb/ft hr)
- C_p = specific heat at constant pressure (But/lb °F)
- H_{fg} = latent heat of vaporization (Btu/lb).

Subscripts f and g denote saturated fluid and steam conditions, respectively.

Selection between Mode 2 and Modes 4, 5, 6 is made by comparing the heat flux with the former mode with the critical heat flux (CHF). In the present logic tree, both departure from nucleate boiling (DNB) and quenching are determined by the same CHF level.

In the two-phase state, GE blowdown CHF correlation[6] is used:

$$\begin{aligned} q_{CHF} &= 10^6\ (0.8 - X) \qquad (G \geq 0.5 \times 10^6) \\ &= 10^6\ (0.84 - X) \qquad (G < 0.5 \times 10^6) \end{aligned} \tag{3.13}$$

where q_{CHF} is critical heat flux (Btu/ft^2 hr), X is quality and G is mass flux (lb/ft^2 hr).

For subcooled water, one from the following three correlations is used depending on the pressure:

Babcock and Wilcox-2 Correlation[7] (used when P > 1500 psi)

$$\begin{aligned} q_{CHF} = {} & \frac{1.5509 - 0.40703(12\mathrm{De})}{12.71\times(3.0545G')^A} \\ & \times \{0.3702\times10^8(0.59137G')^B - 0.15208\times H_{fg}G\} \\ A = {} & 0.71186 + (2.0729\times10^{-4})(P-2000) \\ B = {} & 0.834 + (6.8479\times10^{-4})(P-2000) \end{aligned} \tag{3.14}$$

where $G' = G/10^6$. The corrective term for non-uniform axial power profile in the original correlation was omitted.

Barnet Correlation[8] (used when 1000 < P < 1300)

$$q_{CHF} = 10^6 \times \frac{A + B(H_f - H_{in})}{C + L} \tag{3.15}$$

$$\begin{aligned} A &= 67.45\times D_{HE}^{0.68}\cdot G'^{0.192}(1 - 0.744e^{-6.512D_{HY}G'}) \\ B &= 0.2587D_{HE}^{1.261}\cdot G'^{0.817} \\ C &= 185 \times D_{HY}^{1.415}\cdot G'^{0.212} \end{aligned}$$

where D_{HE} = equivalent diameter for heated surface (in),

$D_{HY} = \sqrt{D_r\ (D_r + D_{HE})} - D_r$ (in),

D_r = fuel rod diameter (in),

L = distance from the inlet (in),

Modified Barnet Correlation[9] (used when P < 725 psi)

Same in form as (3.15), but the coefficients A, B and C are given by

$$A = 73.71 D_{HE}^{0.052} G'^{0.663} (1 - 0.315e^{-11.34 D_{HY} G'})$$

$$B = 0.104 D_{HE}^{1.445} G'^{0.691}$$

$$C = 45.44 D_{HY}^{0.0817} G'^{0.5866}$$

In the pressure range which is not covered by the above three correlations, the critical heat flux is given by the interpolation of the values at the both ends of the range.

3.4 Radiant Heat Transfer

Radiant heat transfer taking place outside fuel rods is described here. First, the rod-to-rod heat transfer is formulated, and the rod-to-coolant heat transfer is treated as a purturbation to the former. Basic assumptions are as follows:

1) each fuel sector surface or shroud element has uniform and independent temperature and emissivity,
2) each axial segment is sufficiently long, so that axial heat tranfer can be neglected.

Under these assumptions, the actual phenomenon is simplified to a two-dimensional radiant heat transfer problem in a vacuum space surrounded by wall elements with different temperatures. Absorption and emission of radiation energy by the coolant can be accounted for by changing the view factors that have been derived under vacuum. The wall elements comprise actual solid surface elements and conceptual symmetry faces, which are treated as completely reflective faces.

To simplify the problem, a third assumption, fictitious this time, is made:

3) the radiation travelling from a subchannel to the next one is converted to isotropic (in hemi-sphere) flux at the boundary.

This assumption enables modular formulation of the problem, i.e., derivation of the heat transfer for the whole bundle cross section from those in subchannels.

3.4.1 View Factors under Vacuum

First, radiant heat transfer in a unit cell is formulated neglecting the presence of coolant. The procedure in this step is described in detail in textbooks of radiant heat transfer[10], hence will be explained only briefly here.

When two faces i and j with areas A_i and A_j are facing each other, the view factor F_{ij} is defined as the fraction of the beams from i that hit face j. A reciprocal relation exists:

$$A_i F_{ij} = A_j F_{ji} \tag{3.16}$$

The view factor is generally obtained by integrating Lambert's equation. But in two-dimensional problem, the procedure is reduced to a simple geometrical relationship, manely cross-string method. In Fig. 9(a), two faces i and j are represented by two lines AB and CD, which are intersections with the cross section. Then changing the definition of A_i to 'area per unit axial length',

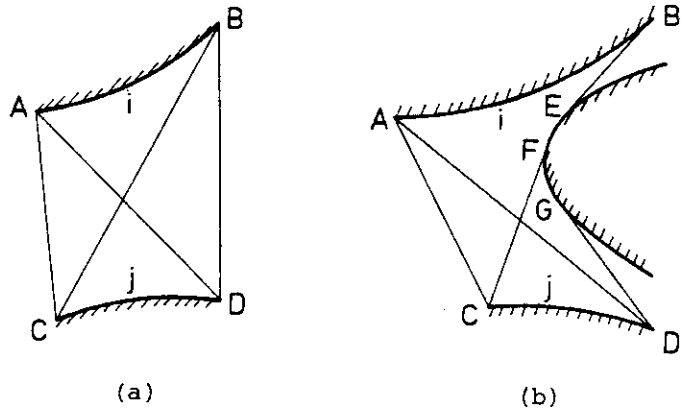

Fig. 9 Cross-string method for geometrical view factors

$$A_i F_{ij} = \frac{1}{2}\,[(AD + BD) - (AC + BD)] \tag{3.17}$$

This relationship of 'diagonal minus lateral' chord length is generalized to the case of Fig. 9(b) where the two faces are partially

hidden by an obstacle. In this case, chords are partially substituted by tangents to the obstacle as shown in the Figure. Chord lengths are calculated using the initial geometry and dimensions of the bundle. Then considering also the part of radiation which reaches face j after multiple reflections, total energy transfer from face i to j is given by

$$E_{ij} = \varepsilon_i \, \varepsilon_j \, \sigma T_i^4 A_i F_{ij}^* = \sigma T_i^4 A_i \psi_{ij} \tag{3.18}$$

where ε is emissivity (= absorptivity), σ is Stefan-Boltzman constant (5.67×10^{-8} J/m^2 s K^4) and T is temperature (K). In (3.18), the term F_{ij}^* has the same meaning as F_{ij} except that reflection is considered, but the definition of ψ_{ij} includes the emissivities ε_i and ε_j of the emitting and absorbing faces.

In a closed space, the following relationships exist for the summation of the view factors from a face to all faces in the space:

$$\sum_j F_{ij} = 1 \tag{3.19}$$

$$\sum_j \psi_{ij} = \varepsilon_i \tag{3.20}$$

The reciprocal relationship of (3.16) applies to F_{ij}^* and ψ_{ij} too.

For calculating the modified view factor ψ_{ij}, another quantity R_{ij} is defined as follows:

R_{ij} = the energy flux leaving face j, when energy flux ε_i from face i (equals the emissivity) is the only radiation source in the space.

From this definition, the following relation between R_{ij} and ψ_{ij} is deduced:

$$A_i \psi_{ij} = A_i R_{ij} \frac{\varepsilon_j}{1 - \varepsilon_j} \tag{3.21}$$

Then noting only the radiation originally emitted from face i, and considering the energy balance among incident, absorbed and reflected energies on face j, the following equation is obtained:

$$(1-\varepsilon_j) \left[\varepsilon_i A_i F_{ij} + \sum_n (A_n R_{in} F_{nj})\right] = A_j R_{ij} \tag{3.22}$$

where the summation in the braket is made on all reflective faces in a unit cell. The first term in the braket means direct incidence from face i to face j. Then still fixing the original emission source to face i, a similar energy balance equation is obtained on the next reflective face $(j+1)$.

Thus, if the total number of reflective faces (total minus boundary faces) in the cell is N', N' set of equations are obtained with N' unknown variables R_{ij}, R_{in} etc. Solving this set of equations for R_{ij}, and applying (3.21) to the results, the modified view factors ψ_{ij} are derived for combinations of face i and the solid faces. For boundary faces on which reflective flux is zero, the following equation is used instead of (3.21):

$$A_i\psi_{im} = \varepsilon_i A_i F_{im} + \sum_n (R_{in}A_n F_{nm}) \tag{3.23}$$

Then the original emission from face $i+1$ is considered, and the same procedure is repeated. The emissions from boundary faces are considered but the symmetry faces are excluded.

Thus modified view factors were determined for all combinations of solid and boundary faces in a unit cell. Using assumption 3), these factors can be easily expanded to the combination of two faces in different unit cells. Let i and j be two solid face elements in two adjacent unit cells having a common boundary face m. Since $A_i\psi_{im}$ is the part of emission from face i that was 'absorbed' at the boundary face m, the flux $A_i\psi_{im}/A_m$ can be regarded as the source term in the next cell. Hence,

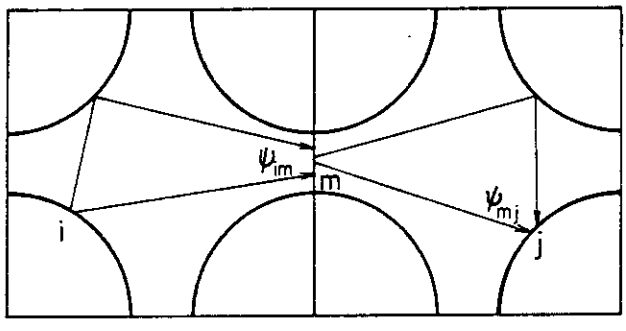

Fig. 10 Connection of modified view factors across boundary faces.

$$A_i\psi_{ij} = (A_i\psi_{im}/A_m)A_m\psi_{mj} = A_i\psi_{im}\psi_{mj} \tag{3.24}$$

Likewise, if faces i and j are separated by two boundary faces m and n,

$$A_i\psi_{ij} = A_i\psi_{im}\psi_{mn}\psi_{nj} \tag{3.25}$$

Practically, however, this cell to cell migration chain cannot be traced until the original emission decays completely. In the code, the number of the chain is limited to two, that is, migrations into adjacent cells and into the further next cells, including the back reflection into the original cell, are considered.

3.4.2 Emission and Absorption by the Coolant

In the foregoing descriptions, the space between solid faces has been assumed to be vacuum. In fact, water absorbs and emits radiation energy even in the steam phase. When the coolant is in the two-phase state, scattering of light by water droplets poses another difficult problem. The FRETA-B treatment of the coolant effect is essentially that for the single-phase steam: the two-phase state is treated simply as an interpolation between steam and completely absorptive fluid states.

When a lump of water vapor exists, an emissivity can be defined for its surface. But different from solid surface case, the emissivity of a vapor lump is not an intrinsic surface property; it depends also on the mass of vapor behind the surface. Several correlations for vapor emissivity have been proposed, out of which FRETA-B uses Schack's equation[11]:

$$\varepsilon_g = \frac{7.0\ (P \cdot L)^{0.8}}{T_g/100} \tag{3.26}$$

where P is pressure (kg/cm), T_g is temperature (°C) and L is the representative dimension of the lump (m).

Emissivity of the two-phase mixture with quality X is approximated by the interpolation between unity (complete absorption) at $X=0$, and the emissivity of the vapor saturated at the pressure $\varepsilon_g(P)$ as

$$\varepsilon = 1 + (\varepsilon_g(P) - 1)X \tag{3.27}$$

As on solid surfaces, emissivity and absorptivity of a vapor lump are identical and complementary to transmissivity:

$$\varepsilon_g = a_g = 1 - \tau_g \tag{3.28}$$

For each travelling of light from face i to j, the fraction of energy lost in the coolant is given by $(a_g)_{ij}$ (equals $(\varepsilon_g)_{ij}$), which is derived from (3.26) taking the representative distance L to be the distance between the centers of the two face elements. Thus the geometrical view factor F_{ij} is replaced by

$$F'_{ij} = F_{ij}\ (\tau_g)_{ij} \tag{3.29}$$

Using F'_{ij} instead of F_{ij}, the procedure of calculating the modified view factors between face elements also applies to the case with the absorption by the coolant. The factors naturally take smaller values than in the vacuum case. Thus instead of (3.20),

$$\sum_j \psi_{ij} < \varepsilon_i \tag{3.30}$$

The difference stands for the energy absorbed by the coolant, so that modified view factor to or from the coolant can be defnined as

$$A_i \cdot \psi_{ik} = A_k \cdot \psi_{ki} = A_i \cdot \varepsilon_i - \sum_j A_i \cdot \psi_{ij} \tag{3.31}$$

where k represents k-th subchannel of the bundle, in which faces i and j are located. It means that the vapor (or two-phase fluid) lump in each subchannel can be treated just as solid face elements. The energy transfer in the opposite direction, emission by the coolant and absorption at a solid face, is also given by (3.18), using $A_k\psi_{ki}$ of (3.31) and taking T_i to be the coolant temperature. The 'connection' of the view factors across boundary faces is made in the same way as between solid faces.

3.4.3 Method of Numerical Calculation

Net radiation energy leaving face i is given by

$$Q_i = \varepsilon_i \sigma A_i T_i^4 - \sum_j (\sigma T_j^4 A_j \psi_{ji}) \tag{3.32}$$

where the summation is made over all relevant solid face elements and vapor lumps (subchannels). Ideally, equation (3.32) should be substituted into the total heat balance equation over the whole bundle, including convective heat transfer and internal heat conduction, and solved simultaneously. But it will make solution of the matrix equation too heavy a process because, in that case, the number of fuel rod radial meshes is multiplied to the size of the matrix. In the code, equation (3.32) is separated from the main thermal calculation routine and the Q_i values are used as the heat source term at the outermost rings of fuel rods in the next time step.

The geometrical view factors $A_i F_{ij}$ are calculated on the initial geometry of the bundle, so that they need calculation only at the start of a transient. But since the modified view factors are affected by the coolant pressure and temperature, they need updating as the transient progresses. This part of calculation is also too heavy a process to repeat every time step. Therefore, the coolant pressure and temperature are monitored at a point in the bundle, and the modified view factors are updated only when the changes from the last updating exceeded threshold values. The thresholds are determined as follows:

1) no updating if void fraction < 0.1,

2) update if void fraction ≥ 0.1, and

$\Delta T_c > 100$ °C $(T_c < 400)$
$\Delta T_c > 50$ °C $(400 \leq T_c < 600)$
$\Delta T_c > 25$ °C $(T_c \geq 600)$

3) update if void fraction ≥ 0.1, and

$\Delta P > 20$ kg/cm^2 $(P > 60)$
$\Delta P > 10$ kg/cm^2 $(20 < P \leq 60)$
$\Delta P > 5$ kg/cm^2 $(P \leq 20)$.

3.5 Heat Conduction in Fuel Rods

One-dimensional heat conduction equation under cylindrical geometry is written in analytical form as

$$\frac{\partial}{\partial t}\left(\rho C_p T(r,t)\right) = \frac{\partial}{\partial r}\left(k \frac{\partial T(r,t)}{\partial r}\right) + S(r,t) \tag{3.33}$$

where ρ is density, C_p is specific heat, k is thermal conductivity and $S(r,t)$ is power density. It is transformed into finite difference form, using central difference for space and Krank-Nicolson method for time. Integrating (3.33) and substituting differential terms with finite differences, the following general form of equation is obtained for radial node point n:

$$a_n T_{n-1}^{m+1} + b_n T_n^{m+1} + c_n T_{n+1}^{m+1} = d_m \tag{3.34}$$

where T_n^{m+1} is the temperature at node n in the new time step $m+1$, and a_n to d_n are coefficients determined by the temperature distribution T^m in the previous time step, and material properties at the temperatures.

Heat transfer at the pellet-clad gap is treated similarly by converting gap conductance to gap thermal conductivity with appropriate 'gap width' g as

$$k' = h_g\, g \tag{3.35}$$

Radiant heat transfer at the pellet-clad gap is nonlinear to temperature. But linear approximation is made by writing the equation in the form:

$$\begin{aligned} q &= A(T_{n+1}^4 - T_n^4) \\ &= A(T_{n+1}^3 + T_{n+1}^2 T_n + T_{n+1} T_n^2 + T_n^3)(T_{n+1} - T_n) \end{aligned} \tag{3.36}$$

where the present time step values are used only in the last linear term, using the known previous-step values for the remaining terms.

Equations of the form (3.34) over a fuel sector are written in matrix form as

$$\begin{vmatrix} b_0 & c_0 & & & \\ a_1 & b_1 & c_1 & & \\ & a_2 & b_2 & c_2 & \\ & & & & \\ & & & & \\ 0 & & & a_{N-1} & b_{N-1} & c_{N-1} \\ & & & & a_N & b_N \end{vmatrix} \begin{vmatrix} T_0^{m+1} \\ T_1^{m+1} \\ T_2^{m+1} \\ \vdots \\ T_{N-1}^{m+1} \\ T_N^{m+1} \end{vmatrix} = \begin{vmatrix} d_0 \\ d_1 \\ d_2 \\ \vdots \\ d_{N-1} \\ d_N \end{vmatrix} \qquad (3.37)$$

where N is the outer surface of the cladding. Making successive elimination from the top down to the N-th line (with suffix $N-1$) of (3.37), we have

$$T_{N-1}^{m+1} + E_{N-1} T_N^{m+1} = F_{N-1} \qquad (3.38)$$

where E_{N-1} and F_{N-1} are coefficients.

The last line of (3.37) is written as

$$a_N T_{N-1}^{m+1} + b_N T_N^{m+1} = d_N \qquad (3.39)$$

It expresses the heat balance in the outermost falf-mesh, and the term d_N contains the surface heat flux q^{m+1}. Solving (3.38) and (3.39), we have an equation of the form:

$$A\ T_N^{m+1} + B = q^{m+1} \qquad (3.40)$$

where T_N^{m+1} is, by the definition, the cladding surface temperature. As stated in 3.4.3, the radiant heat flux is not considered in q^{m+1} here: it is treated as an independent heat source (or sink) term. Hence, another equation relating the surface heat flux to the cladding surface temperature is selected from the convective heat transfer correlations described in 3.3, and written in general form as

$$q^{m+1} = f(T_N^{m+1}) \qquad (3.41)$$

Solving (3.40) and (3.41), we obtain the surface heat flux and the temperature at the outermost radial node. Then following the elimination process of (3.38) backward, temperatures at all radial nodes are derived.

Since this solution procedure is applied successively to each fuel sector, four different values of the center temperature will result for each rod. To avoid this situation, and to account for the heat transfer between fuel sectors, the calculated fuel temperatures at the inner radial nodes are averaged among four sectors. The extent to which this

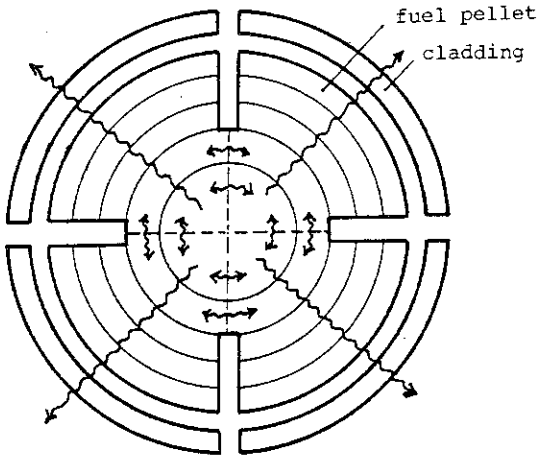

Fig. 11 Treatment of inter-sector heat flow by connecting central rings

averaging is made is specified by the input variable *NFLATT*. For example, if *NFLATT* = 2,

$$T^*_{1,j}(j=1,4) = \frac{1}{4}\,(T_{1,1} + T_{1,2} + T_{1,3} + T_{1,4})$$
$$T^*_{2,j}(j=1,4) = \frac{1}{4}\,(T_{2,1} + T_{2,2} + T_{2,3} + T_{2,4}) \qquad (3.42)$$

where the first subscript denotes radial nodes, and the second one the sector number. The averaged temperatures $T^*_{i,j}$ are used as the old temperature distribution in the next time step, so that repeating this cycle corresponds to calculating heat transfer between fuel sectors. The option *NFLATT* is utilized to adjust the method to various circumstances with different azimuthal temperature gradients.

3.6 Gap Conductance Model and Material Property Data

Heat transfer across the fuel-clad gap takes place by solid-solid contact, heat conduction through gas layer, and radiation. The Ross-Stoute equation, which is originally for the contact case, is modified to include the first two of the above.

With the nominal hot gap size (radial) t_g, gap state is examined as follows:

$$\text{if} \quad t_g > 1.98\ (R_f + R_c), \quad \text{gap is open,}$$

$$\text{if} \quad t_g \leq 1.98\ (R_f + R_c), \quad \text{gap is closed.}$$

where R_f and R_c are the arithmetic mean roughnesses of fuel pellet and the cladding, respectively.

Modified Ross-Stoute equation for gap conductance is

$$h_g = \frac{k_g}{t_0 + (g_1 + g_2)} + h_r \qquad \text{(gap open)} \tag{3.43a}$$

$$= \frac{2\ P_i}{R^{0.5}\ H} + \frac{k_g}{t_0 + (g_1 + g_2)} + h_r \qquad \text{(gap closed)} \tag{3.43b}$$

where h_g = gap conductance (W/cm °C)

k_g = thermal conductivity of the mixed gas (W/cm °C)

H = Mayer hardness of the cladding (kg/cm)

P_i = contact pressure between pellet and cladding (kg/cm)

h_r = radiant gap conductance.

R is the square mean roughness of the fuel and cladding determined by

$$R = \left(\frac{R_f^2 + R_c^2}{2}\right)^{1/2} \tag{3.44}$$

The term t_o is the thickness of gas layer in the roughness, given empirically by

$$t_o = 1.98e^{-0.00125P_i}\ (R_f + R_c) \tag{3.45}$$

The terms g_1 and g_2 are temperature jump distances at the fuel and cladding surfaces, respectively, and the sum of the two is given empirically by

$$g_1 + g_2 = 0.3831\ \left[\frac{\mu}{P}\left(\frac{T + 273}{M}\right)^{1/2}\right] \tag{3.46}$$

where μ is viscosity of the gas (g/cm/s), P is gas pressure (kg/cm^2) T is temperature (°C) and M is the average molecular weight of the gas.

Equation (3.43) assumes that pellets are in concentric position in

the cladding. In fact, even when nominal hot gap is calculated to be open, some of the pellet fragments are making soft contact with the cladding. This effect is accounted for by a fractional relocation model; it is assumed that 10 % of a pellet circumference (or sector circumference) is making a soft contact with the cladding regardless of the hot gap state, whereas the other 90 % remains in the concentric position. Thus the gap heat transfer coefficient is given by

$$h_g = 0.9\ h_g(t_g) + 0.1\ h_g(t_g') \tag{3.47}$$

where $h_g(t_g)$ is the conductance value determined by (3.43a) and t_g' is the soft-contact gap size given by

$$t_g' = 1.98\ (R_f + R_c) \tag{3.48}$$

Thus the transition point from the open to closed gap states is

$$t_g = t_g' = 1.98\ (R_f + R_c) \text{ and } P_i = 0 \tag{3.49}$$

Then equations (3.43a), (3.43b) and (3.47) all give an identical gap conductance value, showing continuous shift of gap state, from open with relocation, to closure with contact pressure.

The gap conductance by radiation is given by the equation for two concentric cylinders:

$$q_r = \sigma\{\frac{1}{\varepsilon_f} + \frac{A_f}{A_c}\ (\frac{1}{\varepsilon_c} - 1)\}^{-1}\{T_f^4 - T_c^4\} \tag{3.50}$$

Linear approximation is made to the above equation in the form of (3.36). Thus the radiant 'gap conductance' is given by

$$h_r = \sigma\{\frac{1}{\varepsilon_f} + \frac{A_f}{A_c}\ (\frac{1}{\varepsilon_c} - 1)\}^{-1}(T_f + T_c)(T_f^2 + T_c^2) \tag{3.51}$$

where σ is Stefan-Boltzman constant, ε is emissivity, A is surface area and T is temperature in the previous time step. Suffices f and c denote fuel and cladding, respectively.

Material properties relevant to the internal heat conduction are specific heats and thermal conductivities of fuel pellet and the cladding, emissivities of fuel and cladding surfaces, and the thermal conductivity

of the mixed gas. MATPRO models are used for most of them.

For thermal conductivity of UO_2 pellet, the Lyons' equation[12] is used with density correction term:

$$k = \frac{1.025}{0.95} \frac{D}{1 + \frac{1}{2}(1-D)} \left(\frac{38.24}{129.4+T} + 6.1256\times10^{-13}\ T^3\right) \qquad (3.52)$$

where k is thermal conductivity (W/cm °C), T is temperature (K) and D is fraction to theoretical density. No correction to the above thermal conductivity is made for circumferential cracking of a pellet.

Thermal conductivity of mix filler gas in fuel rods is calculated from the concentrations of seven gases: helium, argon, krypton, xenon, hydrogen, air and water vapor. Thermal conductivities of each gas component is taken from MATPRO, but the correction for small gap (so called Knudsen domain correction) is not adopted. It is because the effect is already considered in the 'temperature jump distance' of the Ross-Stoute equation.

3.7 Correction for Flow Area Reduction due to Ballooning

Extensive ballooning of the cladding affects the fuel rod thermal states through the changes in the coolant state. FRETA-B treats it as a local purturbation from the input normal flow state, neglecting the effects to the upstream and downstream segments. Large ballooning will start near the center of the core height and propagate towards the both ends. Also radially, it will start from some high temperature rods in a bundle. Thus its primary effect to the coolant will be uneven mass flux distribution among subchannels in the axial segment.

Pressure drop in a subchannel, Δp, over an axial segment is given by

$$\Delta p\ S = \tau\ L\ \ell_w \qquad (3.53)$$

where S is flow area of the subchannel, ℓ_w is wet perimeter, L is the length of the segment, and τ is the shear stress at the wall, which is related to mean flow velocity by

$$\tau = c_f \frac{1}{2} \rho u_m^2 \qquad (3.54)$$

Then

$$\Delta p = \frac{c_f\ \ell_w\ L}{2\ S} \rho\ u_m^2 = \frac{c_f\ \ell_w\ L}{2\ \rho\ S}\ G^2 \qquad (3.55)$$

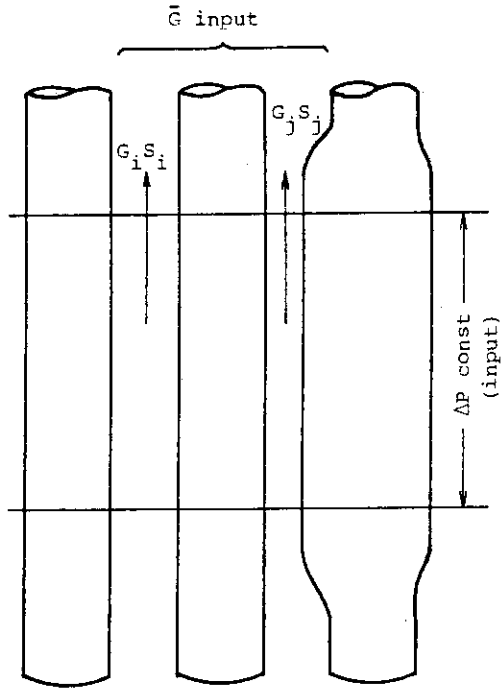

Fig. 12 Re-distribution of input mass flux according to local frictions

where u_m is the mean velocity, ρ is density, and G is mass flux. The friction coefficient c_f is assumed to be constant over all the subchannels, though in fact it depends on the Reynolds number, hence on the local flow state. Then under the condition that the pressure drop between the top and the bottom of the axial segment is the same in all the subchannels, (3.55) leads to

$$G = K\sqrt{\frac{S}{\ell_w}} \tag{3.56}$$

where K is a constant. With the input average mass flux $\bar{G}$, local mass flux in each subchannel is given by

$$G_i = \bar{G}\,\frac{\sqrt{(\frac{S}{\ell_w})_i}\,(\sum_i S_i)}{\sum_i[\sqrt{(\frac{S}{\ell_w})_i}\,S_i]} \tag{3.57}$$

Flow area and wet perimeter are calculated from the fuel rod geometry data, supplied from the mechanical subcode. The geometry of a fuel rod is given in the form,

$$r_i = f(\theta) \tag{3.58}$$

where r_i is the outer surface radius at azimuthal angle θ of rod i. Using the pitch distance 2ℓ, total wet perimeter of a subchannel is given by

$$\ell_w = \sum_i [\int ds_i] \tag{3.59}$$

$$ds_i = \sqrt{r_i'^2 + r_i^2}\, d\theta \qquad (r' = \frac{dr}{d\theta}) \tag{3.60}$$

where the integration is made over a $\pi/2$ span of each rod, and the summation is made over the four rods surrounding the channel.

Likewise, flow area is given by

$$S_i = 4\ell^2 - \sum_i [\frac{1}{2} \int r_i(\theta)^2\, d\theta] \tag{3.61}$$

Use of (3.57) for re-distributing the input mass flux is restricted to the case where the number of the reduced subchannel is small, so that the total flow area in the cross section is not so different from the initial condition.

4. METAL-WATER REACTION MODEL

At high temperature, Zircaloy cladding tubes react with water (steam) in the following mode:

$$Zr + 2\ H_2O \longrightarrow ZrO_2 + 2\ H_2.$$

The zirconia layer forms on the surface, and oxygen diffuses from it into the inner metal phase, raising the concentration there. Oxidation also proceeds from the inner surface after the cladding rupture.

The metal-water reaction is calculated one-dimensionally in each cladding sector if its temperature has exceeded the input threshold value (usually 973 K). Figure 13 shows a model radial distribution of oxygen in the cladding. The alpha-zirconium phase lies next to the oxide layer. Beta zirconium phase may also be present in the inner part if the temperature is high and the oxygen concentration is low. In this model, however, the two phases are not distinguished because the oxygen diffusion constants in them are known to be similar.

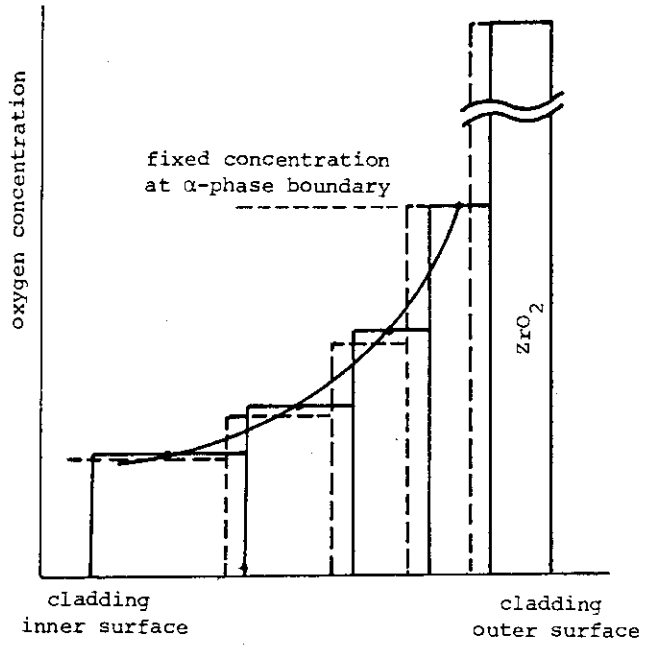

Fig. 13 Moving mesh for treating oxygen diffusion in the cladding. Broken line shows the distribution after adjustment for oxide layer growth

Also for approximation, growth of the oxide layer is calculated by an empirical formula, independently of the oxygen diffusion in the metal phase. The growth rate follows the parabolic reaction rate rule:

$$h^2 = K\ t \tag{4.1}$$

where h is the thickness of oxide layer (cm), and t is time (s). K is a temperature-dependent rate constant given, according to Cathcart[13], by

$$K = 1.13 \times 10^{-2} \exp\left(-\frac{35.9}{RT}\right) \tag{4.2}$$

where R is gas constant (kcal/mol K) and T is temperature (K).
Equation (4.1) is written in incremental form:

$$(h^{m+1})^2 - (h^m)^2 = K\ \ t \tag{4.3}$$

where $m+1$ denotes the present time step whose size is Δt, and m the previous time step. Thus,

$$h^{m+1} = \sqrt{(h^m)^2 + K\ \Delta t} \tag{4.4}$$

Volume increment of the oxide layer in unit axial length is

$$\Delta V = \pi\{(r_0 - h^m)^2 - (r_0 - h^{m+1})^2\} \tag{4.5}$$

where r_0 is the initial outer surface radius. Oxidation from the inner surface is calculated similarly.

Finally, reaction heat, given as follows, is added to linear heat rating of the rod (sector):

$$q_{react} = \rho \cdot \Delta V \cdot Q \tag{4.6}$$

where ρ is the density of the original metal, and Q is reaction heat (6512 J/g-Zircaloy).

Diffusion of oxygen in the metal phase is incrementally calculated every time step using the results of oxidation calculation as boundary condition. Diffusion equation under slab geometry is used:

$$\frac{\partial c}{\partial t} = -D \frac{\partial^2 c}{\partial r^2} \tag{4.7}$$

where c is oxygen concentration (g/cm^3), t is time (s), r is radius (cm), and D is diffusion constant (cm^2/s), which is given by[14]

$$D = 3.923 \exp\left(-\frac{51.0}{RT}\right) \tag{4.8}$$

The metal layer is divided into radial rings with variant thicknesses, finer near the oxide phase and coarser in the interior. The mesh is renewed every time step as oxidation reduces the total thickness of the metal layer.

As in the heat conduction equation, equation (4.7) is transformed into finite difference equation: central difference for space and Krank-Nicolson's method for time derivative are used. Then a set of linear equations is obtained in the following general form for node i:

$$\alpha_{i-1} c_{i-1} + \beta_i \cdot c_i + \gamma_{i+1} \cdot c_{i+1} = \delta_i \tag{4.9}$$

where c_{i-1}, c_i and c_{i+1} are the concentrations in the present time step and the coefficients α to δ are dependent on the concentrations in the previous time step.

Boundary condition at the outer surface is always given by a fixed value of c, i.e., the concentration at the outermost node c_N is set to the equilibrium concentration at the α-Zr/(α-Zr + ZrO_2) phase boundary, which is nearly independent of temperature[15]:

$$c_N = 0.45365 \qquad \text{g/cm}^3$$

On the other hand, the boundary condition at the inner surface (or boundary) is given either by the fixed concentration:

$$c_1 = c_N = 0.45365 \tag{4.10}$$

when the cladding rupture has occurred, or from the no-flux condition:

$$\beta_1' c_1 + \gamma_2' c_2 = \delta_1' \tag{4.11}$$

when the cladding is intact.

In either case, Gauss' elimination procedure is applied to (4.9) from the inner to the outer surfaces. For the i-th ring, the elimination up to c_{i-2} gives an equation of the form:

$$E_{i-1}c_{i-1} + F_i\, c_i = G_i \tag{4.12}$$

From (4.9) and (4.12), new equation fir $(i+1)$-th ring is derived as

$$E_i\, c_i + F_{i+1}\, c_{i+1} = G_{i+1} \tag{4.13}$$

When $i+1$ equals N, the outermost node, c_{i+1} is a known value from the boundary condition, so that (4.13) readily gives the value of c_{N-1}. Then substituting the concentration values successively into the equation set of (4.13) form, the concentrations at all nodes are derived.

Since the total thickness of the metal phase decreases every time step, the radial meshes are renewed at the start of every time step, dividing the residual thickness into constant fractions. Discrete concentration values at the new node points are calculated by linear interpolation of the values at the old nodes.

Average oxygen concentration is calculated in each azimuthal sector from the distribution thus obtained, for use in other subcodes.

5. MECHANICAL MODELS

5.1 Scope

The deformation modes considered in FRETA-B are, thermal expansion of fuel pellets and the cladding, pellet-cladding interaction (PCI), and the cladding deformation due to differential pressure, e.g., ballooning and collapse. Bending of fuel rods, interaction with spacers, and rod-rod mechanical interaction are not modelled in the present version.

Figure 14 shows the flow sheet of mechanical calculation. The subcode DEFORM is separately called for each axial segment. Thermal expansion of fuel pellet is calculated independently in each azimuthal sector. Expansion of the cladding is also determined at one point in each sector, but for the later ballooning calculation, the number of data point is artificially increased by interpolation to 16 or 20 for each rod circumference.

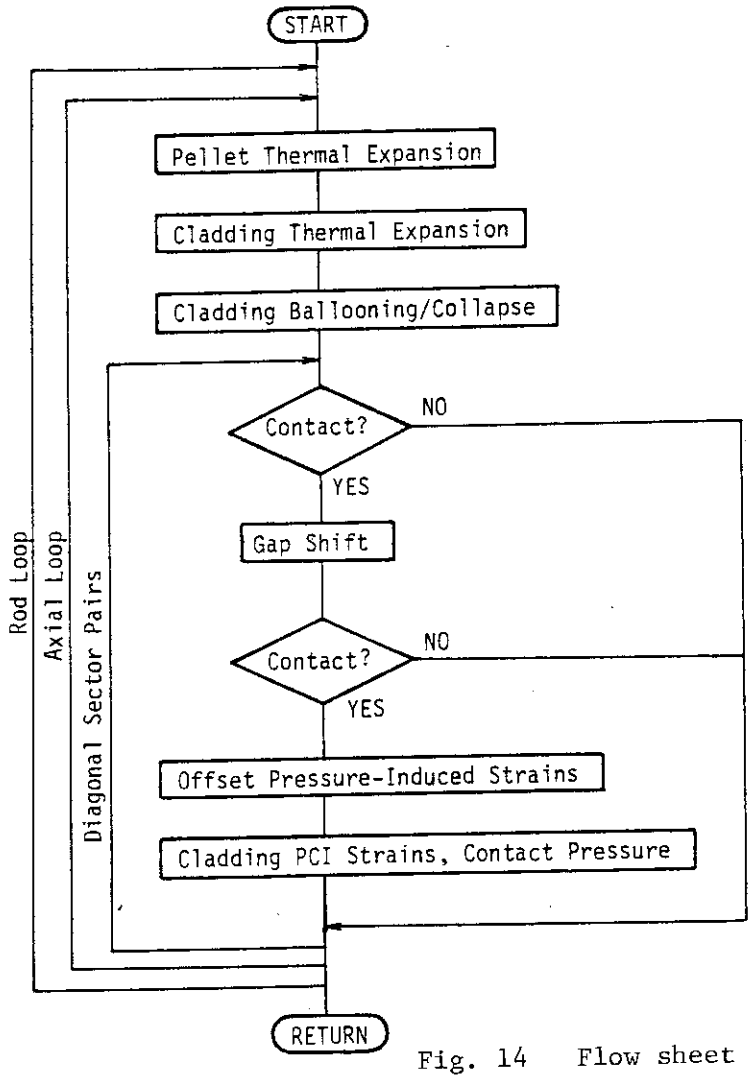

Fig. 14 Flow sheet of the mechanical subcode

The cladding deformation due to hydrostatic pressure difference is calculated in all sectors regardless of the gap state. After that the gap state is examined, and if a gap is closed, the result of the prior calculation is offset and replaced by PCI calculation.

Treatment of the pressure-induced cladding deformation is quasi-two-dimensional: displacements of azimuthal nodes affects each other through the curvature of the midplane profile. Treatment of PCI is not completely independent in each sector: the gap size is averaged between opposite sectors.

The code has a criterion for the cladding rupture taken from MATPRO[3], which compares hoop strains with threshold values. But since the threshold values generally exceed the level at which rod-to-rod contact occurs, the present code simply stops a calculation if displacement at any node has progressed beyond the mid-point of rod-rod spacing.

Thermal expansion coefficients and elastic properties data were mostly taken from MATPRO, whereas the plastic behavior of the cladding is determined by a set of creep equations taken from various sources.

5.2 Thermal Expansions

For calculating overall thermal expansion of a fuel pellet, the effect of cracking must be considered. FRETA-B has two options for its treatment:

MODEXP = 0 ; half-crack model (GAPCON-THERMAL model),
= 1 ; complete-crack model.

In the complete-crack model, the expansion of every radial ring is assumed to be unrestrained, so that the overall expansion is simply given by the sum of local expansions. In the half-crack model, radial cracks are assumed to extend from the outer surface to a radius of the fuel and the expansions in the inner rings are restrained. But this model is used only for the expansion in the radial direction; the complete-crack model is always used in the axial direction.

The unrestrained thermal expansion of each ring is calculated by the MATPRO model, in which linear thermal expansion is expressed as integral length change from a reference temperature to temperature T (K):

$$[UO_2]\ a = -4.972\times10^{-4} + 7.107\times10^{-6}T + 2.581\times10^{-9}T^2 + 1.14\times10^{-13}T^3 \qquad (5.1)$$

$$[PuO_2]\ a = -3.9735\times10^{-4} + 8.4955\times10^{-6}T + 2.151310^{-9}\ T^2 + 3.7143\times10^{-14}T^3 \quad (5.2)$$

Thermal expansion of a mixed oxide is given by the weighted average of the above two a values. Then two quantities ΔR_i and ΔR_i^* are defined in each ring by

$$\Delta R_i = a_i\ \Delta r_i \quad (5.3)$$

$$\Delta R_i^* = a_i \cdot r_i^* \quad (5.4)$$

where Δr_i and r_i^* are the width and the mean radius of ring i, respectively, at the reference temperature.

If MODEXP=0, a ring having the largest value of ΔR_i^* is searched, and (denoting this ring as IB) the radial displacements of the rings are given by

$$u_i = \Delta R_i^* \qquad (i \le IB) \quad (5.5a)$$

$$= u_{IB} + \sum_{j=IB}^{i} \Delta R_j \qquad (IB+1 \le i) \quad (5.5b)$$

If MODEXP=1, for every ring

$$u_i = \sum_{j=1}^{i} \Delta R_j^* \quad (5.6)$$

Outward displacements of the cracked pieces convert the pellet-cladding gap space to crack volumes. Crack volume per unit axial length is given by

$$V_C = 2 \sum_{i=IB}^{NFOP} (u_i - \Delta R_i^*)\Delta r_i(1 + a_i) \quad (5.7)$$

where NFOP is the number of the outermost fuel ring.

The axial expansion in each ring is calculated by multiplying the cumulative thermal expansion ratio a by h_{p0}, the initial pellet height. The fuel stack length change is determined by the axial expansion at a representative radius r_s, which is given by

r_s = radius at dish shoulder (dish pellet),

= radius of the input node (flat pellet),
= 0 (flat pellet and no input).

The initial pellet height at a radius r which is smaller than r_{ds} (dish shoulder radius) is given, in one-end dish case, by

$$h_{d0} = h_{p0} - d + (R - \sqrt{R^2 - r^2}) \tag{5.8}$$

where $R = (r_{ds}^2 + d^2)/2d$, and d is the depth of spherical dish. This h_{d0} is used in place of h_{p0} in the dish region, and the dish volume is calculated by

$$V_{dish} = \sum_{i=1}^{NS-1} \{A_i(h_s - h_d)\} \tag{5.9}$$

where NS is the node number of the representative point, h_s is the pellet height there, and A_i is the cross sectional area of ring i. They are all hot-state values.

All these calculations are made successively in each fuel sector. To calculate total fuel stack elongation, unique value of axial elongation in an axial segment must be determined from the four different values. For simplicity, it is made only by averaging the four values: a representative sector is not determined as in the radial case. Total dish volume is determined simply by adding the volume of (5.9) over all sectors and all axial segments.

As in fuel, only four temperature data are available in a circumference of the cladding, for calculating thermal expansion. But the number of node points is increased to 16 or 20 per circumference for smooth calculation of two-dimensional ballooning. Their temperatures are given by interpolating the four calculated values, using the equation

$$T(\theta) = A_0 + A_1 \sin(\theta) + A_2 \sin(2\theta) + A_3 \cos(\theta) \tag{5.10}$$

where θ is the azimuthal angle measured from a sector boundary, so that the four calculated data are given at $\frac{\pi}{4}$, $\frac{3}{4}\pi$, $\frac{5}{4}\pi$, and $\frac{7}{4}\pi$.

Since the thin-shell model is used in all mechanical models of claddings, thermal expansion is represented by that of the midplane. Thermal expansion coefficient of Zircaloy is texture dependent. In the MATPRO model used in the code, a fixed texture is implicitly assumed and

the integral coefficients from a reference temperature are given separately in axial and radial directions:

$$[\text{axial}] \quad a = \frac{\Delta L}{L_0} = -2.506\times10^{-5} + 4.441\times10^{-6}T \quad (300\ K \le T \le 1073\ K)$$
$$= -8.3\times10^{-3} + 9.7\times10^{-6}\ T \quad (1273\ K \le T) \qquad (5.11)$$

$$[\text{radial}] \quad a = -2.373\times10^{-4} + 6.721\times10^{-6}\ T \ (300\ K \le T \le 1073\ K)$$
$$= -6.8\times10^{-3} + 9.7\times10^{-6}\ T \ (1273\ K \le T) \qquad (5.12)$$

Between 1073 K and 1273 K, which is the two-phase region of unoxidized Zircaloys, discrete data are given as a table.

5.3 Deformation of Cladding due to Pressure Difference

A cladding tube is assumed to be axially uniform in an segment. Hence the treatment of ballooning and collapse is two-dimensional in the transverse direction.

Figure 15 shows the model of non-uniform deformation in a cladding cross section. In each rod, cylindrical coordinate is used with origin at the center of the original geometry. Midplane radius r and wall thickness h in an element of the cladding depends on azimuthal angle θ, expressed by Fourier series every time step:

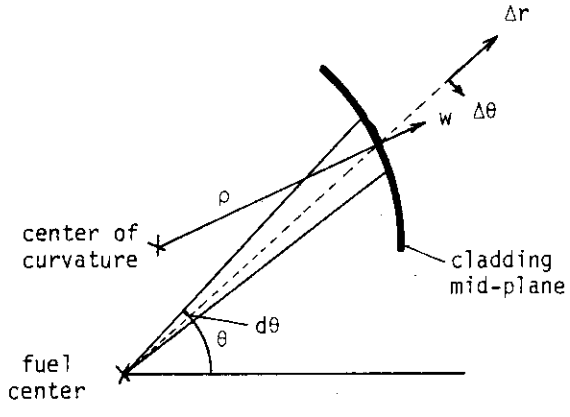

Fig. 15 Local curvature of the cladding midplane

$$r(\theta) = r_0 + \sum_{n=1}^{N} [a_n\cos(n\theta) + b_n\sin(n\theta)] \qquad (5.13)$$

$$h(\theta) = h_0 + \sum_{n=1}^{N} [c_n\cos(n\theta) + d_n\sin(n\theta)] \qquad (5.14)$$

where N is normally taken to 2 or 3. Using abreviations

$$r' = \frac{dr}{d\theta} \quad and \quad r'' = \frac{d}{d\theta}\left(\frac{dr}{d\theta}\right)$$

the curvature at point (r,θ) is given by

$$\frac{1}{\rho} = k = \frac{r^2 + 2r'^2 - r \cdot r''}{(r^2 + r'^2)^{3/2}} \tag{5.15}$$

Here a local coordinate is introduced, which is distinguished from the rodwise cylindrical coordinate by suffices:

local	ρ	..... normal
	t	..... tangential
global (in a rod)	r	..... radial
	θ	..... azimuthal.

Z-axis is common to the two coordinates from the assumption.

With zero curvature in z-direction, the cladding hoop stress is given by the membrane theory as

$$\sigma_t = \frac{\rho \, \Delta p}{h(\theta)} \tag{5.16}$$

where ρ is the radius of curvature and Δp is derived from the rod internal and external pressures p_i and p_o, respectively, as

$$\Delta p = p_i - p_o \tag{5.17}$$

Axial stress is assumed to be constant over a cross section and given by

$$\sigma_z = \frac{P_i \, S_i - P_o(S_i + S_c)}{S_c} \tag{5.18}$$

where S_i is the cross-sectional area of the rod internal volume and S_c is the area of the cladding cross section. They are calculated, using the Fourier expansion (5.13) and (5.14), as

$$\begin{aligned} S_i &= \frac{1}{2}\int_0^{2\pi} [r(\theta) - \frac{1}{2} h(\theta)]^2 d\theta \\ &= (r_o - \frac{h_o}{2})^2 + \frac{\pi}{2} \sum_{n=1}^{N} [(a_n - \frac{c_n}{2})^2 + (b_n + \frac{d_n}{2})^2] \end{aligned} \tag{5.19}$$

$$S_c = 2\, r_0\, h_0 (1 + \varepsilon_\theta^{th})^2 \tag{5.20}$$

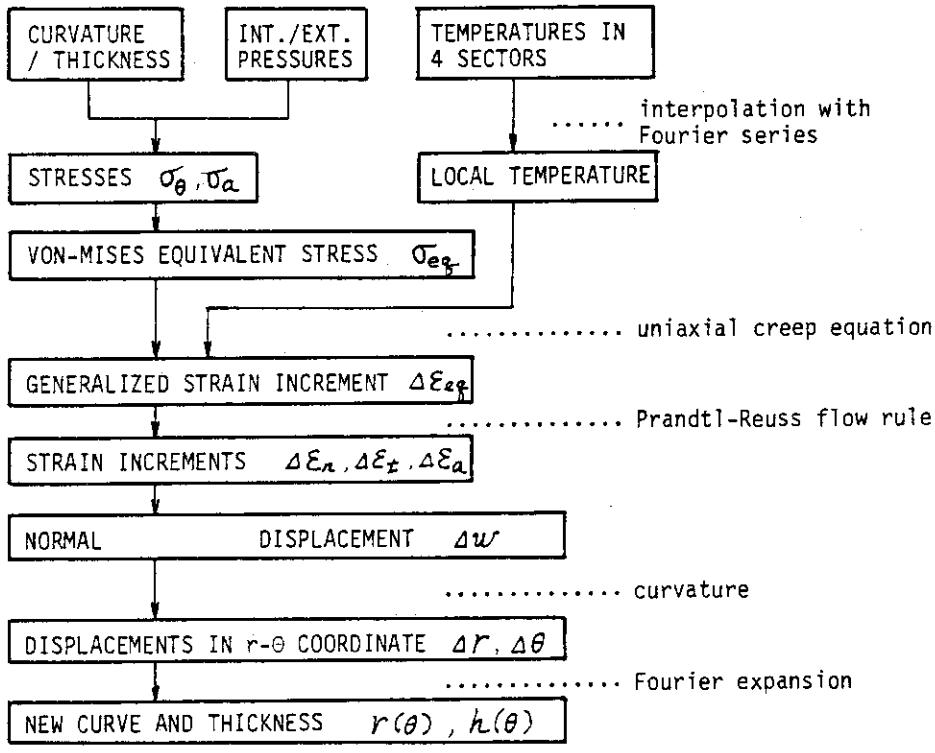

Fig. 16 Flow of two-dimensional ballooning calculation

where ε_θ^{th} is the thermal strain in circumferential direction. Radial stress component is neglected as is usual in the thin-shell model.

Using these stress components, elastic strains are calculated as

$$\begin{aligned} \varepsilon_t^e &= \frac{1}{E}(\sigma_t - \nu\sigma_z) \\ \varepsilon_z^e &= \frac{1}{E}(\sigma_z - \nu\sigma_t) \\ \varepsilon_r^e &= \frac{-\nu}{E}(\sigma_t + \sigma_z) \end{aligned} \tag{5.21}$$

where E and ν are the Young's modulus and Poisson's ratio of Zircaloy, respectively.

With radial stress neglected, von Mises' equivalent stress is given as

$$\sigma_{eq} = (\sigma_t^2 - \sigma_t\sigma_z + \sigma_z^2)^{1/2} \tag{5.22}$$

Using σ_{eq}, equivalent strain increment is calculated by

$$\Delta\varepsilon^{p}_{eq} = \dot{\varepsilon}^{p} \cdot \Delta t = f(\sigma_{eq}) \cdot \Delta t \tag{5.23}$$

where $f(\sigma)$ represents a creep function of Zircaloy, details of which will be described later. Δt is time step size.

Three components of the plastic strain increment are calculated using Prandtl-Reuss flow rule as

$$\Delta\varepsilon^{p}_{i} = \frac{3}{2} \frac{S_i}{\sigma_{eq}} \Delta\varepsilon^{p}_{eq} \tag{5.24}$$

where S_i represents three deviatoric stress components in the local coordinate system.

At the end of the time step, total strain components are derived as

$$\varepsilon_i = \varepsilon^{e}_{i} + (\varepsilon^{p}_{i})_{old} + \Delta\varepsilon^{p}_{i} + \varepsilon^{th}_{i} \tag{5.25}$$

With the strain components, normal and axial components of the cladding local displacement are given by

$$\Delta w_\rho = \rho \ \Delta\varepsilon_t \tag{5.26}$$

$$\Delta L = \Delta z \ \Delta\varepsilon_z \tag{5.27}$$

where Δz is the axial segment length. In this model, displacement in a cross section occurs only along the radius of curvature, so that it has no tangential component.

The normal displacement Δw_ρ is decomposed into (r,θ) components in the rod global coordinate by

$$\Delta r = \frac{r \ \Delta w_\rho}{\sqrt{r'^2 + r^2}} \tag{5.28}$$

$$\Delta\theta = \frac{-r'}{\sqrt{r'^2 + r^2}} \frac{\Delta w_\rho}{r} \tag{5.29}$$

The wall thickness increment is simply given by

$$\Delta h = h \ \Delta\varepsilon_\rho \tag{5.30}$$

Thus, though the increments of strains and displacements are successively calculated at each circumferential nodes, they are not independent of the deformations at other nodes; they affect each other through the curvature of the midplane as calculated from the Fourier series.

At the end of calculations on each rod, new geometry of the cladding is expressed by the following data set:

$$(r_{i,old} + \Delta r_i,\ \theta_{i,old} + \Delta\theta_i,\ h_{i,old} + \Delta h_i)\ \ (i=1 \text{ to } N_\theta) \quad (5.31)$$

It is used as the data set for the Fourier expansion in the next time step. Merit of expressing the geometry by continuous function is that it enables setting of azimuthal nodes always at fixed angles from the fuel center, instead of the nodes built into the material which change the angle seen from the center.

5.4 Pellet-Cladding Interaction

The pellet-cladding gap state and the interaction are calculated at one point in each sector of a rod axial segment. As shown in Fig. 14, the gap state is examined after thermal expansions and the pressure-induced cladding deformation were calculated.

First, the gap state is determined in each fuel sector independently. Open or closed gap state is defined by the sign of the radial gap size given by

$$t_g = r_{CI} - (r_{FO} + \bar{\mu}) \quad (5.32)$$

where $\bar{\mu} = 1.98\ (\mu_f + \mu_c)$,

and r_{CI} and r_{FO} are radii of the cladding inner surface and the fuel outer surface, respectively, and μ is surface roughness with suffices f and c meaning fuel and cladding, respectively. The radius r_{CI} is the value at the center of a sector: the added circumferential nodes for ballooning calculation are not used here.

When t_g is positive in all of four sectors, the gap is open and the result of the prior pressure-deformation calculation is regarded as the final result in the present time step. If, on the other hand, t_g is found to be negative in a fuel sector i, the gap size is averaged between the opposite sectors:

$$\bar{t}_g(i,i+2) = \frac{1}{2}\{(t_g)_i + (t_g)_{i+2}\} \tag{5.33}$$

and the sign of $\bar{t}_g$ is checked again.

Thus gap closure is defined as the state of a couple of fuel sectors diagonal to each other, and PCI is calculated for the couple. The code is prepared to the situation that the gap is closed along one diagonal of a rod, whereas open along the other one.

Even in a general case, the magnitude of interaction is different between two diagonal sector couples. But the interaction in each sector is treated as if it is exisymmetric, to use a simple form of the thin-shell model. The following assumptions are made for simplification:

1) fuel pellet is much more rigid than Zircaloy cladding, so that deflection of pellets can be neglected,
2) PCI is axially uniform in an axial segment and is independent of the conditions in other segments,
3) after contact, no slipping between fuel and the cladding.

From assumption 1), displacement hence strain of the cladding is uniquely determined by the differential thermal expansions of pellets and the cladding. Therefore the purpose of calculating PCI is to derive the contact pressure and the plastic strain increment of the cladding.

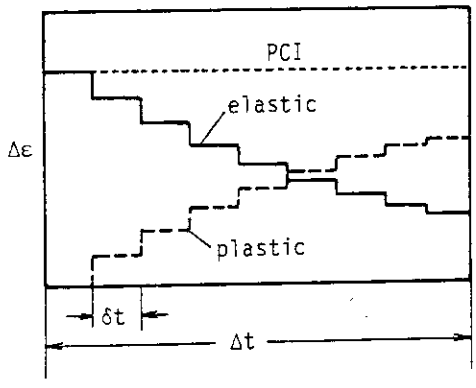

Fig. 17 Stress-relaxation model of PCI strains

The PCI- induced stress-strain history in a time step is treated as a kind of stress relaxation testing with fixed displacement. At the beginning of time step Δt, the excess displacement of pellet is accomodated entirely by elastic straining of the cladding. Then with time, the elastic strain is gradually converted to plastic strain,

reducing the stress. For calculating this process, the given time step size Δt is divided into 2 to 30 sub-steps depending on the magnitude of the initial elastic strain:

$$\Delta t = \delta t_1 + \delta t_2 + \cdots\cdots\cdots + \delta t_N \tag{5.34}$$

From thin shell model and neglecting radial stress again, the elastic strain increments are related to stress increments by

$$\begin{aligned} \Delta\varepsilon_\theta^e &= \frac{1}{E}\,(\Delta\sigma_\theta - \nu\,\Delta\sigma_z) \\ \Delta\varepsilon_z^e &= \frac{1}{E}\,(\Delta\sigma_z - \nu\,\Delta\sigma_\theta) \\ \Delta\varepsilon_r^e &= -\frac{\nu}{E}\,(\Delta\sigma_\theta + \Delta\sigma) \end{aligned} \tag{5.35}$$

From assumption 3), differential deflections of fuel and the cladding, both radial and axial, are known variables after thermal expansions were calculated. They, designated G and H, are related to the cladding strains by

$$G = \Delta\varepsilon^{th}(fuel) - \Delta\varepsilon^{th}(clad) = \Delta\varepsilon_\theta^e - \frac{h}{2\,r_m}\,\Delta\varepsilon_r^e \tag{5.36}$$

$$H = \Delta\varepsilon_z^{th}(fuel) - \Delta\varepsilon_z^{th}(clad) = \Delta\varepsilon_z^e \tag{5.37}$$

where r_m is midplane radius and h is wall thickness of the cladding, and $\Delta\varepsilon_\theta^{th}$ and $\Delta\varepsilon_z^{th}$(fuel) and thermal strain increments at the outer surface of the pellet. The θ and z components are in fact equal.

Substituting (5.35) into (5.36) and (5.37), we obtain

$$\frac{1}{E}\,(\Delta\sigma_\theta - \nu\,\Delta\sigma_z) + \frac{\nu\,h}{2r_m \cdot E}\,(\Delta\sigma_\theta + \Delta\sigma_z) = G \tag{5.38}$$

$$\frac{1}{E}\,(\Delta\sigma_z - \nu\,\Delta\sigma_\theta) = H \tag{5.39}$$

Solving (5.38) and (5.39),

$$\Delta\sigma_\theta = \frac{G + \nu(1-B)H}{(1+\nu)(1-\nu+\nu B)}\,E \tag{5.40}$$

$$\Delta\sigma_z = \frac{G + (1+\nu B)H}{(1+\nu)(1-\nu+\nu B)}\,E \tag{5.41}$$

where $B = \frac{h}{2\, r_m}$

Substituting (5.40) and (5.41) into (5.35), the 'initial' elastic strain of the time step Δt are calculated as

$$\varepsilon_\theta^{e,init} = \frac{(1-\nu^2)G - \nu(1-\nu)BH}{(1+\nu)(1-\nu+\nu B)} + \varepsilon_\theta^{e,old} \tag{5.42}$$

$$\varepsilon_z^{e,init} = \frac{[(1-\nu^2) + \nu(1+\nu)B]H}{(1-\nu)(1-\nu+\nu B)} + \varepsilon_z^{e,old} \tag{5.43}$$

The initial stresses are obtained by adding $\Delta\sigma_\theta$ and $\Delta\sigma_z$ to the corresponding stresses at the end of the previous step. Using these stresses, von Mises' equivalent stress is determined by

$$\sigma_{eq} = (\sigma_\theta{}^2 + \sigma_\theta\sigma_z + \sigma_z{}^2)^{1/2} \tag{5.44}$$

Then, using the uniaxial creep function, the generalized strain increment in the first sub-step δt_1 is calculated. Its components are calculated applying Prandtl-Reuss flow rule, as in the calculation of pressure-induced deformation.

At the end of the sub step δt_1, elastic strains are reduced by the same amount as the plastic strain increments:

$$\delta\, \varepsilon_i^e = -\,\delta\, \varepsilon_i^p \tag{5.45}$$

Then using (5.35), the stress increments (actually reduction) due to relaxation are calculated as

$$\begin{aligned} \delta\, \sigma_\theta &= \frac{E}{1-\nu^2}\,(\delta\varepsilon_\theta^e + \nu\delta\varepsilon_z^e) \\ \delta\, \sigma_z &= \frac{E}{1-\nu^2}\,(\delta\varepsilon_z^e + \nu\delta\varepsilon^e) \end{aligned} \tag{5.46}$$

and subtracted from the 'initial' stresses.
The procedure from (5.44) to (5.46) is repeated in subsequent sub-steps to the last one $\delta\, t_N$, and the stress components and the strain components, both elastic and plastic, are finally determined as the end state of the whole time step Δt as

$$\sigma_i = \sigma_i^{old} + \Delta\sigma_i^{init} - \sum_j^N (\Delta\varepsilon_i)_j \tag{5.47}$$

$$\varepsilon_i^e = \varepsilon_i^{old} + \Delta\varepsilon_i^{e,init} - \sum_j^N (\delta\varepsilon_i^e)_j \tag{5.48}$$

$$\varepsilon_i^p = \varepsilon_i^{p,old} + \sum_j (\delta\varepsilon_i^p)_j \tag{5.49}$$

The pellet-cladding contact pressure is calculated by

$$P_c = \frac{r_{CO}P_o + h\,\sigma_\theta}{r_{CI}} - P_i \tag{5.50}$$

Different from the pressure-induced deformation case, the PCI deformation of the cladding is evaluated at one point in each fuel sector. The derived displacement is uniformly allocated to all the added circumferential node points in the sector. Thus the Fourier series fitting of the midplane locus is made with the same number of circumferential data points along the circumference. Therefore, the state of partial PCI, open gap along one diagonal and closed gap along the other, can be treated with no difficulty in algorism.

5.5 Stress-Strain Constitutive Equation of Zircaloy

In both of the pressure-induced and PCI-induced cladding deformations, the calculation procedure of plastic strain increment was to apply a creep-type function to the von-Mises' equivalent stress. In fact, the plastic behavior of Zircaloy in the beta-phase and in the high-temperature range of the alpha phase is suited for the creep type of formulation: strain rate is given as an explicit function of stress, with small strain hardening considered as the primary creep term. But in the low temperature range of the alpha phase, where strain hardening is dominant in determining the strain increment, the constitutive equation is given, not in the creep form, but in the plasticity form. The whole temperature range is divided into four ranges: 1) low-temperature range of the alpha-phase, 2) high-temperature range of the alpha-phase, 3) two-phase range, and 4) beta-phase range. Between 1) and 2), discontinuity is unavoidable. Stress and strain are both expressed by true stress and strain, respectively. Zircaloy-2 and Zircaloy-4 are not distinguished.

low-temperature range of alpha-phase (T < 900 K)

The MATPRO-09 model[3] is used with small modifications. The constitutive equation is written in the form:

$$\sigma = K\,\varepsilon^{n} \tag{5.51}$$

where σ is stress (MN/m^2), and ε denotes here total strain including both elastic and plastic components, and K and n are constants determined by temperature, cold work and fast neutron fluence.

$$K = (1.075\times10^{3} - 0.9996\cdot T)\cdot(1 - 0.546w) \tag{5.52}$$

$$n = (-0.0186 + 7.11\times10^{-4}\,T - 7.721\times10^{-7}\,T^{2})\cdot Y\cdot Z \tag{5.53}$$

$$Y = 0.847\,\exp(-39.2w) + 0.153 - 0.0916w + 0.229w^{2}$$

$$Z = \exp[-(\phi t)^{1/3} / (3.73\times10^{7} + 2\times10^{8}\,w)]$$

where T is temperature (K), w is cold work (m^2/m^2), ϕ is the fast neutron flux (n/m^2 s) and t is time (s).

For calculating the plastic strain increment, yielding of the material must be checked. It is made by comparing the strains ε_1 and ε_2, which are determined by the new stress σ and the old plastic strain ε^{p}_{old} as

$$\varepsilon_1 = \varepsilon^{p}_{old} + \frac{\sigma}{E}$$

$$\varepsilon_2 = \left(\frac{\sigma}{E}\right)^{1/n} \tag{5.54}$$

and if $\varepsilon_1 \geq \varepsilon_2$, the material is elastic and $\varepsilon = \varepsilon_1$,
if $\varepsilon_1 \leq \varepsilon_2$, the material is plastic and $\varepsilon = \varepsilon_2$,

In the first case, there is no plastic strain increment, whereas in the second case, the increment is given by

$$\Delta\varepsilon^{p} = \varepsilon - \varepsilon^{p}_{old} \tag{5.55}$$

High-temperature range of the alpha-phase (900K ≤ T ≤ 1093K)

Clay-Redding's secondary creep equation[16] is used with the Garofalo-type primary creep term, as proposed in CANSWEL model[17]:

$$\dot{\varepsilon}^{p} = \dot{\varepsilon}^{ps}\{(1 + 1.8\,\exp(-30\varepsilon^{p})\}$$

$$\dot{\varepsilon}^{ps} = 2920\,\sigma^{5}\,\exp\left(-\frac{34508}{T}\right) \tag{5.56}$$

where σ is stress (MN/m^2). In the original CANSWEL model, the strain in the primary creep term of (5.56) was 'accumulated secondary creep strain'. It was changed to the total plastic strain ε^p for simplicity, and the numerical constant was also changed accordingly based on some internal testing data.

Beta-phase range (1253K < T)

Clendening's secondary creep equation[18] is used without primary creep term. With the same units for stress and temperature,

$$\dot{\varepsilon}^p = 24\ \sigma^{3.7}\ \exp\left(-\frac{18220}{T}\right) \tag{5.57}$$

The two-phase range (1093K < T < 1253K)

The complex superplastic behavior of Zircaloy has not yet been fully elucidated. Hence the constitutive equation in this range is simply given by interpolation of the equations of alpha-, and beta-phases with the following assumptions:

1) volumetric compositions of the two phases are determined only by the present temperature,
2) external load is borne by the internal stresses in the two phases according to their compositions,
3) the strains in the two phases induced by the internal stresses are equal in amount.

Assuming linear dependency on temperature, volumetric fractions of the two phases are given by

$$\begin{aligned} V_\alpha &= (1253 - T)/160 \\ V_\beta &= 1 - V_\alpha \end{aligned} \tag{5.58}$$

From assumption 2),

$$\sigma = V_\alpha\ \sigma_\alpha + V_\beta\ \sigma_\beta \tag{5.59}$$

and from assumption 3), using (5.56) and (5.57) for the internal stresses,

$$\dot{\varepsilon}^p = 2920\ \sigma_\alpha{}^5\ \exp\left(-\frac{34508}{T}\right) = 24\ \sigma_\beta{}^{3.7}\ \exp\left(-\frac{18220}{T}\right) \tag{5.60}$$

where the primary creep term was omitted from the alpha-phase equation.

Equations (5.59) and (5.60) are simultaneously solved by a numerical procedure for given T and σ, and the plastic strain rate is obtained.

6. FUEL ROD INTERNAL GAS PRESSURE MODELS

The gas pressure at the cold state is input: as a transient code, FRETA-B relies on other codes for estimating the amount of fission gas released into the plenum during steady operations. The code calculates the gas pressure at the hot state, and optionally transient gas flow through the pellet-cladding gap. Naturally fuel rods are not divided into azimuthal sectors in the pressure calculation, but free volumes in the four sectors, calculated in other subcodes, are summed in each axial segment or in a rod.

6.1 Uniform Gas Pressure in a Rod

If not specified the opposite by input, the gas pressure in a fuel rod is regarded uniform in every part. Free volumes considered are: upper and lower (if any) plena, fuel-clad gap, center hole, dish, and crack volume of fuel pellets. Ideal gas law is applied to each volume element:

$$P\ V_i = n_i\ R\ T_i \tag{6.1}$$

where P is pressure, R is gas constant, and V_i, n_i, T_i are the volume, gas moles, and the local temperature of volume element i. Volume element is set for each category of void volume and for each axial segment. Smaller volume elements in fuel radial rings and azimuthal sectors are summed into axial-segmentwise volume elements. The mean temperature of each volume element is decided as follows:

1) upper and lower plenum temperatures are set equal to the outlet and inlet coolant temperatures, respectively,
2) pellet-clad gap temperature is given by the average of the fuel and cladding surface temperatures. Sectorwise values are averaged.
3) the temperature at fuel crack volumes is given by the volumetric average temperature of fuel, whereas the temperatures at center hole, dish volumes are given by respective representative temperatures. Sectorwise values are averaged.

Plenum volumes are reduced by differential thermal expansion between fuel stack and cladding. The upper plenum volume is calculated by:

$$V_{pu} = V_{pu0} \left(1 - \delta \frac{\Delta h}{L_{pu0}}\right) \tag{6.2}$$

where L_{pu0} and V_{pu0} are the length and volume, respectively, of the upper plenum in the cold state, and Δh is the differential thermal expansion. Depending on the lower end geometry,

$\delta = 1$ (no lower plenum),

$\delta = \frac{1}{2}$ (with lower plenum).

The hot volume of the lower plenum, if any, is given by (6.2) with δ equals 1/2, i.e., when plena exist at both ends, the fuel stack elongation is assumed to be accomodated equally at the both ends. Again, the stack elongation is averaged over four azimuthal sectors.

Equation (6.1) is written in the form:

$$\left(\frac{V}{T}\right)_i = n_i \frac{R}{P} \tag{6.3}$$

Since gas pressure is uniform all over a fuel rod, (6.3) can be summed over whole void volumes. Hence,

$$P = n R / \sum_i \left(\frac{V}{T}\right)_i \tag{6.4}$$

where n is the total gas moles in a rod.

When the cladding has ruptured at an elevation, the gas pressure is instantaneously set equal to the current external pressure.

6.2 Transient Pressure Gradient and Axial Gas Flow

Transient axial gas pressure gradient in a rod arises from the resistance to the gas flow from the plena to a fuel stack part where temperature or void volume has drastically changed. The gas flow path consists of the pellet-cladding gap and fuel cracks. Relocation of fuel fragments converts the concentric gap space to complex crack volumes. Rigorous modelling of the gas flow path is difficult under this complex geometry. Therefore, an approximation is made that the fuel stack is in the concentric position without relocation, and that the resultant uniform gap space is the only gas flow path, deviation from the actual geometry being considered by adjusting a numerical constant according to experimental data.

The plenum gas is regarded as Piseulle fluid, i.e., laminar flow with zero velocity at the solid walls. Thus the phenomenon is idealized as a typical hydrodynamic problem in a closed space. But standard procedures for treating such problems are not used here because of the following stability-related problems:

1) since the flow and mass-balance equation is non-linear, the Krank-Nicolson's semi-explict solution cannot be used,
2) implicit solution, or explict solution with fine time meshing is time consuming, and
3) the objective of calculating gas flow is to derive pressure gradients under large flow resistances, not to derive gas flows under small flow resistances.

Thus the problem is treated by switching between uniform-pressure, and pressure-gradient assumptions depending on the instantaneous and local stability.

The molecular gas flow through an annular part from position $i+1$ to i is given by

$$F = \frac{\pi\, g^3\, r \cdot (P_{i+1}^2 - P_i^2)}{12 \mu R T \ell} \tag{6.5}$$

where F is flow rate (moles/s), g and r are the width and the mean radius of the annulus, respectively, P is pressure, μ is viscosity, and ℓ is the distance between the two positions.

Equation (6.5) transforms to the form:

$$F \cdot R^f = P_{i+1}^2 - P_i^2 \tag{6.6}$$

where

$$R^f = \frac{12\, \mu R\, T\, \ell}{\pi\, g^3\, r} \tag{6.7}$$

Giving the variables in (6.7) the average values in axial segment i, the flow resistance between two ends of the segment, R_i^f, can be determined. The resistance between the centers of the segments i and $i+1$ is given by

$$R_{i,i+1}^f = \frac{1}{2} (R_i^f + R_{i+1}^f) \tag{6.8}$$

Then (6.6) can be modified to relate the gas flow rate to the square pressure difference between axial segments i and $i+1$:

$$R^f_{i,i+1} \cdot F_{i+1,i} = P^2_{i+1} - P^2_i \tag{6.9}$$

where $F_{i+1,i}$ is molecular gas flow rate from segment $i+1$ to segment i (moles/s). Here an implicit approximation has been made that the flow resistance between two segments is 'concentrated' at the boundary.

The gas mole increase in unit time in segment i is given by

$$\Delta n_i = \left[\frac{P^2_{i+1} - P^2_i}{R^f_{i,i+1}} + \frac{P^2_{i-1} - P^2_i}{R^f_{i,i-1}}\right] \Delta t \tag{6.10}$$

The explict method of solution is to apply (6.10) successively to all the axial segments including the plenum and, using the old time step values of pressure and flow resistance, to calculate the gas mole increment in each segment and finally to derive new pressure values by the ideal gas law.

But by this method, a stability problem arises when either gas mole inventory is small in a segment, or the flow resistance is small (gap size is large), or the time step size is large. To circumvent this problem, a stability check is made in each segment successively from the lower end using a factor defined by

$$f = \frac{\Delta t}{n \cdot R^f} \tag{6.11}$$

First, the gas mole inventory and flow resistance of the lowest segment, n_1 and R^f_1, are substituted to (6.11) together with the current time step size. If the resultant f value is greater than a limiting value which is currently 10^{-7} $(\text{Mpa})^{-2}$, the stability of the segment is judged to be insufficient. Then, the first and the second segments are integrated into a single gas volume having a uniform pressure. The flow resistances and gas moles are summed over the two segments and the factor f is determined for the integrated volume by (6.11). This procedure is repeated until, after integration of segments 1 to j, the f-factor is small enough.

Thus the first integrated gas volume, which comprises segments 1 to j, has been determined, and integration into the next one is started from segment $j+1$ upward in the same way. The last gas volume includes the

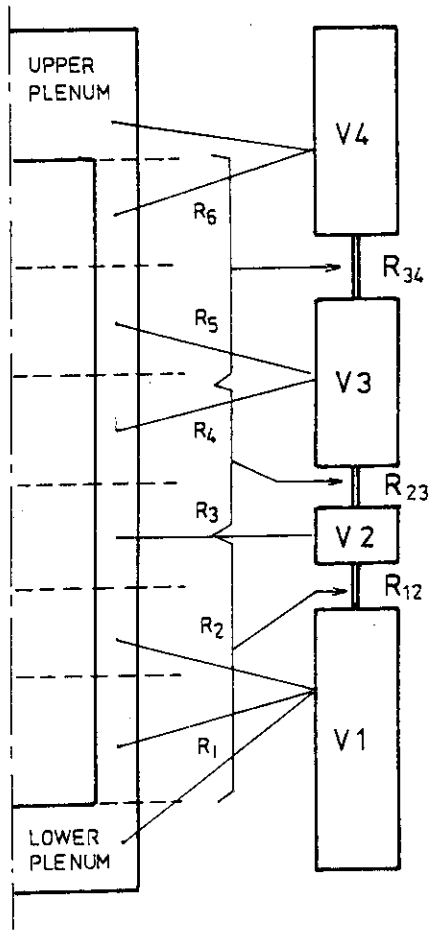

Fig. 18 Integration of axial segments into uniform-pressure volumes

upper plenum. The number of the integrated volumes M differs from time step to step. When the pellet-cladding gap size is large in every axial segment, all the segments and plena are integrated into a signle gas volume, that is, the uniform pressure option in temporarily adopted.

When the number of the integrated volumes is not unity, the pressure in each volume V_m (m equals 1 to M) is calculated as in the case of uniform gas pressure over a rod, namely, summation of V/T over all the segments that belong to V_m. Also the inter-segment flow resistance given by (6.8) is replaced by inter-integrated-volume resistances. Then the gas mole balance equation (6.9) is applied to the flow between the integrated volumes. From the results, the pressure in V_m at the end of the time step is obtained as:

$$P_m = (n_m + \Delta n_m)R \;/\; \sum_{i\ m} \left(\frac{V}{T}\right)_i \tag{6.12}$$

Since the pressure P_m is common to all segments which belong to V_m, the segmentwise gas inventory is calculated by

$$n_i = P_m \left(\frac{V}{T}\right)_i / R \tag{6.13}$$

The above procedure was in fact a method for calculating gas flow through idealized concentric pellet-cladding gap. More generally, equation (6.5) can be written in the form:

$$F = \frac{\pi}{Ha} \bar{D} \cdot D_H \frac{P_{i+1}^2 - P_i^2}{2\mu RT\ell} \tag{6.14}$$

where $\bar{D}$ is the midplane diameter of the flow path, D_H is equivalent hydraulic diameter and Ha is a numerical constant called Hagen number. Equations of the form (6.14) can universally treat the flows in annular paths and cylindrical tubes. In the present annular flow case,

$$\begin{aligned} \bar{D} &= 2r \\ D_H &= 2g \\ Ha &= 96. \end{aligned} \tag{6.15}$$

The actual complex geometry of the flow path is considered by changing the Ha number. According to an experiment[19], the Ha number is at least 200. The number is left as an input option with a standard value of 200.

7. CONCLUSION

The calculation runs of FRETA-B for verification are now under way. The results will be published in separate papers.

A key point in expanding the previous FRETA code into a multi-rod version was to avoid much increase in necessary core memory space and calculation time. This line has been kept through the development work up to the present version. The already-performed verification runs have shown that the calculation times, when divided by the total number of node points, are similar to those by the previous single-rod version.

It was accomplished by the limited use of two-dimensional treatment as well as frequent use of explicit solution method. But at the same time, those verification runs have also shown that the thermal model requires still more two-dimensional treatments: the assumption of uniform coolant temperature in all subchannels of a bundle (cross section) requires modification. To enrich these models avoiding excessive burden on calculation time is the next task.

The present code has some inconsistencies between submodels, e.g., neglect of the cladding oxide layer in thermal and mechanical calculations. The amendments of these inconsistencies will be undertaken in the development work to the next version.

ACKNOWLEDGEMENT

The authors are grateful to Dr. M. Nozawa, Head, Division of Reactor Safety, for his encouragement of the work. They also acknowledge valuable advices by Dr. M. Ichikawa, Head, and Mr. M. Suzuki of Fuel Reliability Lab. I.

7. CONCLUSION

The calculation runs of FRETA-B for verification are now under way. The results will be published in separate papers.

A key point in expanding the previous FRETA code into a multi-rod version was to avoid much increase in necessary core memory space and calculation time. This line has been kept through the development work up to the present version. The already-performed verification runs have shown that the calculation times, when divided by the total number of node points, are similar to those by the previous single-rod version.

It was accomplished by the limited use of two-dimensional treatment as well as frequent use of explicit solution method. But at the same time, those verification runs have also shown that the thermal model requires still more two-dimensional treatments: the assumption of uniform coolant temperature in all subchannels of a bundle (cross section) requires modification. To enrich these models avoiding excessive burden on calculation time is the next task.

The present code has some inconsistencies between submodels, e.g., neglect of the cladding oxide layer in thermal and mechanical calculations. The amendments of these inconsistencies will be undertaken in the development work to the next version.

ACKNOWLEDGEMENT

The authors are grateful to Dr. M. Nozawa, Head, Division of Reactor Safety, for his encouragement of the work. They also acknowledge valuable advices by Dr. M. Ichikawa, Head, and Mr. M. Suzuki of Fuel Reliability Lab. I.

REFERENCES

(1) Uchida, M., Harayama, Y., and Otsubo, N.: "FREG-3T: A computer program to analyze LWR fuel behavior under accident conditions", JAERI-M 8482 (1979). (in Japanese)

(2) Katsuma, K.R. et al.: "RELAP4/MOD5: A computer program for transient thermal-hydraulic analysis of nuclear reactors and related systems", ANCR-NUREG-1335 (1976).

(3) MacDonald, P.E. and Thompson, L.B., "MATPRO-VERSION 09: A handbook of materials properties for use in the analysis of lighe water reactor fuel rod behavior", TREE-NUREG-1005 (1976).

(4) Chung, H.M. and Kassner, T.F.: "Deformation characteristics of Zircaloy cladding in vacuum and steam under transient-heating conditions: summary report", ANL-77-31 (1978).

(5) Revised ANS Standard (ANS 5.1) "Decay heat power in light water reactors for shutdown times less than 10^4 seconds", (1978).

(6) Slifer, B.C., Hench, J.E.: "Loss-of-coolant accident and emergency core cooling models for General Electric boiling water reactors", NEDO-10329 (1971).

(7) Gellerstedt, J.S. et al.: "Correlation of critical heat flux in a bundle cooled by pressurized water", Two-Phase Flow and Heat Transfer in Rod Bundles, paper presented at ASME symposium, Los-Angels, (Nov. 1969) pp.63-71.

(8) Barnett, P.G.: "A Correlation of Burnout Data for Uniformly Heated Annuli and Its Use for Predicting Burnout in Uniformly Heated Rod Bundles", AEEW-R463 (1966).

(9) Hughes, E.D.: "A correlation of rod bundle critical heat flux for water in the pressure range 150 to 725 psia", IN-1412 (1970).

(10) Hottel, H.C.: "Radiant heat transmission", Chapter 4 or "Heat Transmission" (ed. McAdams, W.H.) McGraw-Hill, (1954).

(11) Schack, A. Arch. Eisen Hüttenwesen, 241 (1939).

(12) Lyons, M.F. et al.: "UO_2 pellet thermal conductivity from Irradiation with central melting", GEAP-5591 (1964).

(13) Cathcart, J.V.: "Zirconium metal-water oxidation kinetics", ORNL/NUGEG/TM-41 (1976).

(14) Pawel, R.E.: "Oxygen diffusion in oxide and alpha Zircaloy Phases", ORNL/NUREG-5, (1976) pp.14.

(15) Domagala, R.F. and McPherson, D.J.: Trans. AIME. 200 (1954) 238.

(16) Clay, B.D., and Redding, G.B.: "Creep properties of alpha-phase Zircaloy-2 cladding relevant to the loss of coolant accident", RD/B/N3187 (1975).

(17) Jones, P.M., Gittus, J.H. and Hindle, E.D.: "CANSWEL: A computer model of clad behaviour during a loss-of-coolant accident", TRG Report 2901(s) (1976).

(18) Clendening, W.R.: "Primary and secondary creep properties for Zircaloy cladding at elevated temperatures of interest in accident analysis", 3rd International Conference on Structural Mechanics in Reactor Technology, London (1975), Vol.1, C2/6.

(19) Dagbjartsson, S.J. et al.: "Axial gas flow in irradiated PWR fuel rods", TREE-NUREG-1158 (1977).

APPENDIX INPUT MANUAL

One FRETA-B run treats one transient event with a set of initial condition data and time-dependent data. The input data classified into five groups with different formats, configurated in the following order:

1) Title Card Format(20A4)
2) NAMELIST /NAM1/
   Mainly single variables are input. Most variables have stored standard values, so that users can specify only those variables which they wish to change from the standard values. Some /NAM1/ data specify the sizes of the array data to be input in the subsequent groups.
3) NAMELIST /NAM2/
   Array data.
4) Fixed-Format Card Group 1
   This group specifies how the bundle in problem is constructed from subchannels and face elements.
5) Fixed-Format Card Group 2
   This group is optional, being used only when it is specified in /NAM1/. It is meant for easy inputting of voluminous coolant condition history data, and can be input either from logical terminal number 5 (card) or from 30 (disc or tape).

(1) Namelist Card Groups

Namelists /NAM1/ and /NAM2/ are given in Tables A1 and A2, respectively. For some variables, users are referred to the example in Table A5. The /NAM1/ variables are classified into 10 groups in Table A1, but it is only for convenience of tabulation. As standard namelist grammer tells, the order in the Table has nothing to do with the actual configuration on input cards.

(2) Fixed-Format Card Group 1

This group of cards are necessary if KRADC = 1 in /NAM1/. The option means that radiant heat transfer is to be calculated. But in the FRETA-B logic, KRADC must always be unity when a bundle geometry (multiple rods) is analyzed, and the configuration of channel and face elements is specified by this group. Users are referred to Chapter 2 of the main text for the definitions of the terms used here.

This card group specifies the correspondence between sequential numbers of fuel rods, subchannels and face elements.

First, all subchannels in a (partial) bundle are given sequential numbers in arbitrary order.

Second, all fuel rods in the (partial) bundle including those intersected by symmetry faces are given sequential numbers also in arbitrary order.

Third, azimuthal sectors in each rod are given numbers 1 to 4 in counter-clockwise sequence (top view). The number 1 can be given to an arbitrary sector including one which is completely outside a symmetry face. Here an azimuthal sector always means a qurter of a rod, even if a symmetry face cuts the sector to two halves.

Fourth, all face elements forming the partial bundle are given sequential numbers. In this case, face elements outside the symmetry face must be omitted. The total number of the face elements must equal the NSURF value in /NAM1/. In this sequence, fuel rod surface elements must come first, and next, other solid faces follow. Then symmetry face elements and boundary faces follow in this or the opposite order. The order in each face group can be arbitrary.

Fifth, for each face element, the type of the coolant subchannel geometry and the position in the channel type to which the face element in problem corresponds, must be identified. Five subchannel types are prepared in the present version, and their numbers and local face numbers are shown in Fig. 7.

The variables and their formats of this card group are explained in Table A3. In addition, an example is given in Table A5 using a simple bundle geometry of Fig. 6.

(3) Fixed-Format Card Group 2

This card group is necessary only when MODSHT equals 5 and ICTAPE equals 5 or 30. It serves for easy inputting of voluminous coolant state history data supplied from other hydrodynamic codes or experimental data records.

If ICTAPE=5, this card group is input by cards, as other card groups.

If ICTAPE=30, the data are input from the logical terminal number 30, which is allocated to either disc or tape.

The array name of this group is a two-dimansional array TVSCT(I,J), which represent time, coolant pressure, mass flux and enthalpy depending

on the I value. Their configuration and formats are shown in Table A4. NTVSCT sets, as input in /NAM1/, of data must be input. In each set, the first card specifies the time, and then a card in each axial mode block, as specified by JCCND data in /NAM1/, gives the local coolant condition data.

Table A1

NAMELIST /NAM1/

Name	Description	Stored Value
	[GROUP 1] Fuel Geometry Data (common to all rods)	
TEMPO	Initial fuel temperature. The following dimensional data are defined at this temperature. (°C)	25.0
RFIP	Fuel inner radius (cm)	0.0
RFOP	Fuel pellet outer radius (cm)	0.46597
RCIP	Cladding inner radius (cm)	0.47422
RCOP	Cladding outer radius (cm)	0.53594
HPELT	Fuel pellet height (cm)	1.5
ZFUEL	Fuel stack height (cm)	365.76
ZCLAD	Cladding length (cm), Not necessary when VPLNUϕ is input.	0.0
DDEPTH	Pellet dish depth (cm) For one-end dish, negative value is input.	0.0
RDISH	Dish shoulder radius (cm) Axial thermal expansion of the pellet stack is estimated at this radius.	0.0
FRDEN	Fuel pellet density (fraction to theoretical density)	0.95
PITCH	Fuel rod to rod pitch (cm)	1.43
DEQ	Equivalent hydraulic diameter of the coolant channel (cm) If not input, calculated from PITCH.	0.0
FAREA	Coolant flow area (cm^2) If zero, calculated from PITCH.	0.0
ROUF	Arithmetic mean roughness of pellet (cm)	0.0004
ROUC	Arithmetic mean roughness of cladding (cm)	0.0002
	[GROUP 2] Material Data	
FRPUO2	Fraction of PuO_2 in fuel pellet	0.0

Table A1

NAMELIST /NAM1/ (cont'd)

Name	Description	Stored Value
MATCLD	Cladding material: = 2 (Zircaloy-2) = 4 (Zircaloy-4)	4
COLDW	Cold work of the cladding (cm^2/cm^2)	0.2
TMELT	Melting point of fuel (°C)	2800.0
	[GROUP 3] Plenum Gas Data	
VPLNUϕ	Upper plenum volume (cm^3). If zero, calculated from other dimensional data.	0.0
VPLNLϕ	Lower plenum volume at TPLEN (cm^3)	0.0
TPLEN(N), N=1,NROD	Initial plenum temperature (°C)	25.0
GASPRS(N) N=1,NROD	Plenum gas pressure at TPLEN (kg/cc). If zero, calculated from GASMOL.	0.0
GASMOL(N) N=1,NROD	Gas moles in each fuel rod. Not necessary when GASPRS ≠ 0.	0.0
GASMIX(N,N) J=1,7 N=1,NROD	Composition of plenum gas. (volume fraction) GASMIX(1) = Helium GASMIX(5) = Hydrogen GASMIX(2) = Argon GASMIX(6) = Air GASMIX(3) = Krypton GASMIX(7) = Vapor GASMIX(4) = Xenon	1.0, 6×0.0
	[GROUP 4] Space Mesh Data	
NOCHAN	Number of coolant subchannels.	1 (≤20)
NROD	Number of fuel rods.	1 (≤10)
NSURF	Total number of solid face elements. Not necessary when radiant heat transfer is not calculated.	0 (≤80)

Table A1

NAMELIST /NAM1/ (cont'd)

Name	Description	Stored Value
NAXIN	Number of axial segments of fuel rods. Exclude upper and lower plena. When segments with different lengths are required, input a negative value.	1 (≤10)
NODF	Number of radial rings in a fuel pellet sector.	5
NODC	Number of radial rings in a cladding sector. (NODF + NODC ≤ 9)	2
NODS	The radial ring number at which the axial expansion of fuel column is determined. If zero, the expansion is calculated at dish shoulder radius. If RDISH is also zero, RFOP/2 is used.	0
NDIV	Option for radial mesh in fuel pellet. NDIV = 0 rings with equal thickness NDIV = 1 rings with equal mass (volume)	1
NBPOIN	Number of circumferential meshes in ballooning calculation. Either 4, or 12, or 20.	12
NFLATT	The radial ring number from which inward, temperatures are averaged among four circumferential sectors.	1
NFORDR	Maximum order of Fourier series in the ballooning calculation. (< NBPOIN/2-1)	2
NSYMSF	Number of fuel sector outside the partial bundle whose state is refered to the state of a symmetrical sector inside the partial bundle. Omit in the single-rod case. In the Fig. 6 case, NSYMSF = 6.	0
	[GROUP 5] Time Step and Power Data	
TIMEϕ	The initial time of transient calculation (s)	0.0
TMAX	The duration of the transient (s) (end time - TIMEϕ)	0.0

Table A1

NAMELIST /NAM1/ (cont'd)

Name	Description	Stored Value
DT	Uniform time step size (s). Omit if time step size is time dependent.	0.01
NTSTP	Length of time step size vs. time table (TVSDT) to be input in /NAM2/. Omit if DT is used.	1
DTSFMX	Maximum allowable jump of the caldding temperature in a time step (°C)	6.0
POWERϕ(N) N=1,NROD	The average linear heat rating of rod N at TIMEO (w/cm). The term $\bar{P}_0(n)$ of eqn. (3.3).	0.0
BURNO	The average burnup at TIMEO (MWD/MTM)	0.0
NPOWER	Length of the average power vs. time table (POWER) to be input in /NAM2/, or option switch about power data. NPOWER > 0 POWER(2,J), J=1,NPOWER are input in /NAM2/. NPOWER = -1 ANS standard table (+20 %) is used. NPOWER = -2 Modified Shure's equation plus delayed fission heat.	0 (<101)
NRPOW	Option of radial power gradient data. NRPOW = 0 radially uniform power generation. NRPOW = 1 FRPDR(2,J), J=1,NRPOW are input in /NAM2/.	0
FRTPW(L,N) L=1,4 N=1,NROD	Relative powers of all fuel sectors of rod N The term f (θ,n) of eqn. (3.3) in the main text.	1.0
RSCRAM	Scram reactivity of the reactor. Used when NPOWER = -2.	0.03
[GROUP 6] Coolant Condition Data		
MODSHT	Option for setting the boundary condition in thermal calculation. MODSHT = 1 Cladding temperature history is input	1

Table A1

NAMELIST /NAM1/ (cont'd)

<table>
<tr><th>Name</th><th>Description</th><th>Stored Value</th></tr>
<tr><td></td><td>
MODSHT = 2 Average coolant condition history is input.
= 3 Coolant history is input at the inlet and outlet.
= 4 Local heat transfer coefficient history is input.
= 5 Local coolant condition history is input.
Dependent on this option, following data must be input in /NAM1/ and /NAM2/:
<table>
<tr><th></th><th></th><th colspan="5">MODSHT</th></tr>
<tr><th></th><th></th><th>1</th><th>2</th><th>3</th><th>4</th><th>5</th></tr>
<tr><td>NAM1</td><td>MINTPC</td><td>○</td><td></td><td></td><td>○</td><td>○</td></tr>
<tr><td></td><td>JCCND</td><td>○</td><td></td><td></td><td>○</td><td>○</td></tr>
<tr><td></td><td>ICTAPE</td><td></td><td></td><td></td><td></td><td>○</td></tr>
<tr><td>NAM2</td><td>TVSCT</td><td>○</td><td></td><td></td><td>○</td><td>○</td></tr>
<tr><td></td><td>TCMFL</td><td></td><td>○</td><td>○</td><td></td><td></td></tr>
<tr><td></td><td>TVHIN</td><td></td><td>△</td><td>△</td><td></td><td></td></tr>
<tr><td></td><td>TVHOT</td><td></td><td>△</td><td>△</td><td></td><td></td></tr>
<tr><td></td><td>TVHAV</td><td></td><td>○</td><td></td><td></td><td></td></tr>
<tr><td></td><td>TVCPRS</td><td>○</td><td>○</td><td>○</td><td>○</td><td></td></tr>
</table>
△ : Only the smaller one out of TVHIN, TVHOT requires accurate data. Input a large value to the other one.
</td><td></td></tr>
<tr><td>NCPRS</td><td>Length of the coolant pressure table (TVCPRS).</td><td>1 (<101)</td></tr>
<tr><td>NMFL</td><td>Length of the coolant mass flux table (TVMFL).</td><td>1 (<101)</td></tr>
<tr><td>NHIN</td><td>Length of the coolant inlet enthalpy table (TVHIN).</td><td>0 (<101)</td></tr>
<tr><td>NHOT</td><td>Length of the coolant outlet enthalpy table (TVHOT).</td><td>0 (<101)</td></tr>
<tr><td>NHAV</td><td>Length of the coolant average enthalpy table (TVHAV).</td><td>0 (<101)</td></tr>
<tr><td>NTVSCT</td><td>Length of the coolant condition table (TVSCT).</td><td>0 (<101)</td></tr>
</table>

Table A1

NAMELIST /NAM1/ (cont'd)

Name	Description	Stored Value
MINTPC	(Omit if MODSHT = 2 or 3.) The coolant condition or cladding temperature data need not be specified at all axial segments. For unspecified segments, these data are determined either blockwise or by linear interpolation accoding to the JCCND data: MINTPC = 0 blockwise data are input, = 1 linear interpolation is made.	
JCCND(20)	(Omit if MODSHT = 2 or 3.) Dependent on MINTPC, the axial segment numbers either at the ends of coolant data blocks, or of the positions at which the data are specified. 1) When MINTPC = 0 (example) When the total number of axial segments is 9, and the same conditions can be assumed in the segments 1 to 3, 4 to 5, and 6 to 9, JCCND = 3, 5, 9. 2) When MINTPC = 1 (example) When the coolant data are available only at segments 1, 4 and 9, JCCND = 1, 4, 9. For other segments, linear interpolation is made.	
ICTAPE	Necessary only when MODSHT = 5. Since the option MODSHT = 5 generally requires voluminous coolant data, user can either input these data in the namelist /NAM2/, or as fixed-format data at the end by card, disc, or tape. ICTAPE = 0 TVSCT data are input in /NAM2/. ICTAPE = 5 TVSCT data are input at the end in fixed format.	0

Table A1

NAMELIST /NAM1/ (cont'd)

Name	Description	Stored Value
	ICTAPE = 30 same as ICTAPE = 5, but either disc or tape is used through the logical machine number 30 (READ(30)).	
	[GROUP 7] Miscellaneous Data and Options	
IOPTGF	Option for transient gas flow calculation. = 0 uniform pressure in a fuel rod, = 1 pressure gradient and gas flow are calculated.	0
KRADC	Option for radiant heat transfer calculation. = 1 calculated, = 0 not calculated. If KRADC = 1, detailed bundle geometry must be input in fixed format after /NAM2/. In multi-rod cases, KRADC must be unity.	1
ICNTCT	= 0 pellet-clad contact is not anticipated at TIMEϕ, = 1 pellet-clad contact is anticipated. If ICNTCT = 1, the initial condition of transient is calculated with smaller time step size.	0
KFLBLK	Option of the coolant subchannel reduction calculation: = 0 not made, = 1 made.	0
TLOWMW	Temperature above which metal-water reaction is calculated (°C).	700.0
RATEMW	Reaction heat of metal-water reaction (J/g-Zr)	6512.0
COEFMW(J) J=1,2	Coefficients of weight-gain equation for metal-water reaction: $W = A_1 \exp(- A_2/R\,T)$ A_1 = COEFMW(1) ($(g\text{-}Zr)^2/cm^4\ s$) A_2 = COEFMW(2) (cal/mole)	1.13×10^{-2} 35900.0

Table A1

NAMELIST /NAM1/ (cont'd)

Name	Description	Stored Value
HAINP	Hagen number in transient gas flow calculation.	200.0
MODEXP	Option for pellet thermal expansion calculation, = 0 half-crack model, = 1 complete-crack model.	1
	[GROUP 8] Data for Output Control Output of transient calculation is made by three subroutines PRIN2D, PRINT1, and PRINT2, which can be used optionally: PRIN2D outputs the results all over the bundle in standard format. PRINT1 makes PRIN2D type output at selected sectors of selected rods, but in all axial segments. It makes printout of radial temperature distribution. PRINT2 makes history-table type printout at selected locations on some key variables. User can choose either or both of PRIN2D and PRINT1 printouts. The number of PRINT2 output is fixed to 200 points over the entire calculation time.	
KPRINT	chooses either or both of PRIN2D and PRINT1: KPRINT = 01 PRIN2D is used, KPRINT = 10 PRINT1 is used, KPRINT = 11 both are used.	01
NTPRIN	Total number of printouts with PRIN2D: NTPRIN = 0 output at 1 s interval if TPRINT(1)=0, output at t s interval if TPRINT(1)=t, NTPRIN = n output at times specified in /NAM2/ by TPRINT(I),I=1, n.	1 (<51)
NTPRN1	Same as NTPRIN, but controls PRINT1 output.	0 (<51)

Table A1

NAMELIST /NAM1/ (cont'd)

Name	Description	Stored Value
NPRP1(I) I=1,10	Specifies the nodes at which PRINT1 output is made. NPRP1(I) = n × 100 + 1 n = rod number, 1 = circumferential sector number	
KPRHIS	Option for selecting key parameters in PRINT2 output: KPRHIS = 0 mainly thermal parameters, = 1 mainly mechanical parameters.	0
NPRHIS(I) I=1,10	Specifies the nodes at which history table output is made by PRINT2. NPRHIS(I) = n × 100 + j × 10 + 1 n = rod number j = axial segment number 1 = circumferential sector number. NPRHIS(I) also specifies the nodes from which the plotting data are taken when IPLOT = 1.	
[GROUP 9] Specifies Plotter Format		
IPLOT	Option for plotter output: = 0 no plotter output, = 1 plotter output.	0
WXAX	Length of X-axis (mm).	150.0
WYAX	Length of Y-axis (mm).	200.0
TBLX(I) I=1,3	TBLX(1) = minimum value of X-axis (s), TBLX(2) = maximum value of X-axis (s), TBLX(3) = interval at which the scale is indicated on X-axis (s).	0.0 50.0 10.0
IPLOTM(I) I=1,13	Specifies the variables to be plotted. IPLOTM(I) = 0 variable I is not plotted, = 1 variable I is plotted, = -1 variable I is superimposed on the previous plot,	13 × 1

Table A1

NAMELIST /NAM1/ (cont'd)

Name	Description	Stored Value
	where 13 variables are as follows: 1 linear heat rating (W/cm) 2 cladding outer temperature (°C) 3 cladding inner temperature (°C) 4 fuel outer temperature (°C) 5 fuel inner temperature (°C) 6 coolant temperature (°C) 7 coolant quality 8 convective heat transfer coefficient (W/cm^2 °C) 9 cladding total hoop strain 10 cladding plastic hoop strain 11 cladding plastic axial strain 12 rod inner pressure (kg/cm^2) 13 coolant pressure (kg/cm^2).	
TBLY(3,I) I=1,13	TBLY(1,I) = Y-axis minimum value of variable I, TBLY(2,I) = Y-axis maximum value of variable I, TBLY(3,I) = Y-axis scaling interval of variable I. These three data are input in the unit of variable I shown in parentheses in the description of IPLOTM(I).	

Table A2 In spacial array data, the argument symbols are used in the meaning: L=sector, J=axial segment, N=rod.

NAMELIST /NAM2/

Array Name	Description
HL(J) J=1,-NAXIN	Length of axial segments (cm). Necessary only when NAXIN < 0.
HOXID(I,L,J,N) I=1,2 L=1,4 J=1,NAXIN N=1,NROD	Initial thickness of the cladding oxide layer (mm). Not necessary if zero. I = 1 inner surface, I = 2 outer surface.
DSWEL(L,J,N) L=1,4 J=1,NAXIN N=1,NROD	Initial displacement of pellet outer surface (cm). Swelling and densification during steady operation can be accounted for by this input. Not necessary if zero.
EPSϕ(K,L,J,N) K=1,3 L=1,NBPOIN J=1,NAXIN N=1,NROD	Initial permanent strain (except plastic strain) of the cladding. K = 1 hoop, K = 2 axial, K = 3 radial Not necessary if zero.
EPSPϕ(K,L,J,N)	Initial plastic strain of the cladding. Meanings of parameters are the same as EPSϕ. Not necessary if zero. Strains of EPSPϕ are considered in strain hardening calculation, but EPSϕ strains are not.
TVSDT(I,J) I=1,2 J=1,NTSTP	Time step size table. Not necessary if NTSTP = 0. TVSDT(1,J) = time (s) TVSDT(2,J) = time step size (s).
TPRINT(I) I=1,NTPRIN	Time when PRIN2D output is made (s). The start and the end states of transient are always output without specifying here. See NTPRIN description in /NAM1/.
TPRIN1(J) J=1,NTPRIN1	Same as TPRINT(J), but controls PRINT1 output.
POWER(I,J) I=1,2 J=1,NPOWER	Bundle average power history table. POWER(1,J) = time (s) POWER(2,J) = power fraction. When POWERϕ ≠ 0, POWER(2,J) is multiplied to POWERϕ. When POWERϕ = 0, POWER(2,J) must be input in absolute value (W/cm).

Table A2

NAMELIST /NAM2/ (cont'd)

Array Name	Description
FAPPO(J) J=1,NAXIN	Axial power distribution (fraction). Normalization is not necessary.
FRPDR(K,I) K=1,2 I=1,NRPOW	Radial power distribution table in fuel pellet. FRPDR(1,I) = radius (cm) FRPDR(2,I) = power density (fraction). Normalization is not necessary.
TVCPRS(K,I) K=1,2 I=1,NCPRS	Coolant pressure history table. TCVPRS(1,I) = time (s) TCVPRS(2,I) = pressure (kg/cm^2)
TVMFL(K,I) K=1,2 I=1,NMFL	Coolant mass flux history table. TVMFL(1,I) = time (s) TVMFL(2,I) = mass flux (kg/m^2 s)
TVHIN(K,I) K=1,2 I=1,NHIN	Coolant inlet enthalpy history table. TVHIN(1,I) = time (s) TVHIN(2,I) = enthalpy (J/kg)
TVHOT(K,I) K=1,2 I=1,NHOT	Coolant outlet enthaply history table. TVHOT(1,I) = time (s) TVHOT(2,I) = enthalpy (J/kg) The smaller one out of TVHIN and TVHOT must be given accurate values, but the larger one only needs an arbitrary value which indicates that it is larger than the other.
TVHAV(K,I) K=1,2 I=1,NHAV	Coolant average enthalpy history table. TVHAV(1,I) = time (s) TVHAV(2,I) = enthalpy (J/kg)
TVSCT(K,I) I=1,NTVSCT	Boundary condition history table. Necessary only when MODSHT = 1, 4, and 5. If MODSHT = 5 and ICTAPE ≠ 0, TVSCT data are input not here but at the end in fixed format. TVSCT data represent different arrays depending on the value of MODSHT. Following abbreviations are used for explanation: t_i = time (s), T_s = cladding surface temperature (°C), T_c = coolant temp. (°C).

Table A2

NAMELIST /NAM2/ (cont'd)

Array Name	Description
	h = heat thansfer coefficient (W/cm^2 °C), p = coolant pressure (kg/cm^2), G = mass flux (kg/m^2 s), H = enthalpy (J/kg). ◦ MODSHT = 1 TVSCT(1,1) = t_1 TVSCT(2,1) = T_s ..... axial block 1 (up to JCCND(1)) TVSCT(3,1) = T_s ..... axial block 2 (up to JCCND(2)) TVSCT(n,1) = T_s ..... axial block n (up to JCCND(n)) TVSCT(1,2) = t_2 TVSCT(2,2) = T_s ..... axial block 1 TVSCT(n,2) = T_s ..... axial block n ◦ MODSHT = 4 TVSCT(1,1) = t_1 TVSCT(2,1) = T_c TVSCT(3,1) = h ..... axial block 1 TVSCT(4,1) = T_c TVSCT(5,1) = h ..... axial block 2 TVSCT(1,2) = t_2 TVSCT(2,2) = T_c TVSCT(3,2) = h ..... axial block 1 ◦ MODSHT = 5 TVSCT(1,1) = t_1 TVSCT(2,1) = p TVSCT(3,1) = G TVSCT(4,1) = H ..... axial block 1 TVSCT(5,1) = p TVSCT(6,1) = G TVSCT(7,1) = H ..... axial block 2 TVSCT(1,2) = t_2 TVSCT(2,2) = p TVSCT(3,2) = G TVSCT(4,2) = H ..... axial block 1

Table A3

Fixed-Format Card Group 1 Radiant Heat Transfer Data

Omit if KRADC = 0.

Card	Column	Variable	Description
Channel Data (NOCHAN cards are successively input.)			
1	1 - 3		Comment field
	4 - 10	ITYP(I)	Channel type number
	11 - 15	ISUF(1,I)	Global face number of local face number 1 in channel 1
	16 - 20	ISUF(2,I)	Global face number of local face number 2 in channel 2
	.	.	.
	.	.	.
	.	.	.
	46 - 50	ISUF(8,I)	Global face number of local face number 8 in channel 1
Face Element Data (For fuel rod surfaces, one card is necessary for each face element. For other faces, one card is required for each category.)			
2	1 - 5	NSF1	First global face number.
	6 - 10	NSF2	Second global face number, Same data are allocated to face elements from NSF1 to NSF2. If zero, set equal to NSF1.
	11 - 15	MATER	Category number of the face element group: MATER = 0 symmetry face, = 1 structural component surface, = 2 fuel rod surface, = 3 boundary between subchannels.
	16 - 20	IROD(1,J)	Necessary only for fuel rod surface elements.
	21 - 25	IROD(2,J)	IROD specifies the fuel rod node number to which global face number J corresponds. IROD(1,J) = circumferential sector number, IROD(2,J) = rod number. (axially uniform)
	26 - 35	EMISSF	emissivity of the face group

Table A3

(cont'd)

Card	Column	Variable	Description
			Data of fuel rod surface elements outside the symmetry faces. Omit if NSYMSF = 0. This card group specifies, from symmetry, which fuel sector outside the partial bundle is identical to which fuel sector inside. Input NSYMSF sets of data in FORMAT(16(1x,I2,2I1)).
3	1		Comment field
	2 - 3	ISYMSF(1,1)	Rod number
	4	ISYMSF(2,1)	Fuel sector number outside the symmetry face
	5	ISYMSF(3,1)	Fuel sector number with which ISYMSF(2,1) is symmetrical.
	6		Comment field
	7 - 8	ISYMSF(1,2)	Rod number
	9	ISYMSF(2,2)	Fuel sector number outside the symmetry face
	10	ISYMSF(3,2)	Fuel sector number with which ISYMSF(2,2) is symmetrical.
	.	.	.
	.	.	.
	.	.	.
	.	.	.
	.	.	.

Table A4

Fixed-Format Card Group 2 Coolant Condition Data

Card	Format	Variable		
1	E10.0	TVSCT(1,1)	time (s) (first data point)	
1a	E10.0	TVSCT(2,1)	coolant pressure (kg/cm^2)	first axial block (JCCND(1))
	E10.0	TVSCT(3,1)	mass flux (kg/m^2 s)	
	E10.0	TVSCT(4,1)	enthalpy (J/g)	
1b	E10.0	TVSCT(5,1)	coolant pressure	second axial block (JCCND(2))
	E10.0	TVSCT(6,1)	mass flux	
	E10.0	TVSCT(7,1)	enthalpy	
⋮				
1n	E10.0	TVSCT(k,1)	coolant pressure	top axial block (JCCND(i))
	E10.0	TVSCT(ℓ,1)	mass flux	
	E10.0	TVSCT(m,1)	enthalpy	
2	E10.0	TVSCT(1,2)	time (second data point)	
2a	E10.0	TVSCT(2,2)	coolant pressure	
	⋮	⋮		
⋮				
n	E10.0	TVSCT(1,n)	time (n-th data point)	
na	E10.0	TVSCT(2,n)	coolant pressure	
	⋮	⋮		
⋮				
nm	E10.0	TVSCT(m,n)	enthalpy	

Table A5 Sample input list (for the geometry, see Figs. 6 and 7.)

```
 BUNDLE TEST ASS.8017
&NAM1   RFOP=0.460,RCIP=0.4740,RCOP=0.536,RDISH=0.0,
HPELT=2.0,ZFUEL=90.0,VPLNUO=3*25.0,GASPRS=3*50.0,
PITCH=1.43,POWERO=3*0.24,
TMAX=60.0,DT=0.50,
DTSFMX=6.0,
NOCHAN=3,NROD=3,NSURF=14,NAXIN=-3,
RELOCT=0.0,NRPOW=0,
NPOWER=18,NCPRS=1,NMFL=1,NHIN=1,NHOT=4,
NTPRIN=5,
NTPRN1=1,
NPRHIS=10202,10203,20201,0,0,0,0,0,0,0,
KPRINT=01,KPRHIS=0,ICNTCT=0,KRADC=1,NSYMSF=6,
MODSHT=3,
NTSTP=4,
&END
&NAM2    FAPPO=3*1.0,
TPRINT=0.0,5.,10.,15.,25.,
TPRIN1=120.,
HL=44.9,20.0,25.1,
TVCPRS=0.0,1.0,
TVMFL=0.0,0.947,
TVHIN=0.0,3.052E+6,
TVHOT=0.0,3.072E+6, 30.,3.072E+6, 100.,3.486E+6, 120.,3.486E+6,
POWER=0.0,1.0, 17.,1.0, 22.,20.2, 24.,29.2, 32.,88.0, 42.,88.000000000
44.,97.2, 50.,102.8, 58.,102.8, 60.,91.5, 73.,91.5, 76.,110.7000000000
84.,110.7, 86.,112.4, 96.,112.4, 98.,33.6, 100.,0.0, 120.,0.0000000000
TVSDT=0.0,1.0, 15.0,1.0, 17.0,0.5, 120.0,0.5,
&END
CH1      2   13    1    3    9   14    7
CH2      3    2   10   13    6    4   11
CH3      1    5   14   12    8
    1         2    2    1        .75
    2         2    3    1        .75
    3         2    1    2        .75
    4         2    4    2        .75
    5         2    2    2        .75
    6         2    2    3        .75
    7    8    1                  .90
    9   12    0
   13   14    3
 0112 0143 0231 0332 0312 0342
----*----1----*----2----*----3----*----4----*----5----*----6-
```

channel data

fuel rod surface elements

shroud face

symmetry face

boundary face

symmetry relationship